576110

Sandia National Laboratories
Waste Isolation Pilot Plant

Analysis Report on Mineral Fragment Colloids under WIPP Relevant Conditions

Work Carried Out under the Analysis Plan for the Experimental Investigation of Stability of Mineral Colloids Under WIPP Conditions, AP-187, Rev. 0.
To be included in the AP-187 records package

Authors:	____*Signature on File*___ Priya Hora, Org. 08882	09/28/2021 Date
	Chammi Miller Chammi Miller, Org. 08882	09/28/2021 Date
	____*Signature on File*___ Jay Jang, Org. 08882	09/28/2021 Date
	Luzheng Zhang, Org. 08882	09/28/2021 Date
	____*Signature on File*___ Leslie Kirkes, Org. 08882	09/28/2021 Date
Technical Reviewer:	Sungtae Kim Sungtae Kim, Org. 08881	9-28-2021 Date
QA Reviewer:	Shelly R. Nielsen Shelly R. Nielsen, Org. 08880	9-28-2021 Date
Management Reviewer:	Antonio Triventi, Org. 08882	9/28/2021 Date

WIPP:4.4.2.2.1:TD:QA-[illegible]
Information Only

42 **Table of Contents**

43 List of Figures 4
44 List of Tables 6
45 Acronyms and Abbreviations 7
46 1 Introduction 9
47 2 Methods for analysis of stability experiments 9
48 2.1 Aggregation kinetics 10
49 2.1.1 Time resolved concentration data 10
50 2.1.1.1 Data fitting 10
51 2.2 Particle size distributions and particle concentration/number 10
52 3 Results and conclusions 11
53 3.1 Estimate of particle settling kinetics 11
54 3.1.1 Task 1 – Analysis of strontianite colloidal stability 12
55 3.1.2 Task 2 – Analysis of calcite colloidal stability 13
56 3.1.3 Estimating settling times and average particle size for Tasks 1 and 2 13
57 3.1.4 Conclusions from settling rates for Tasks 1 and 2 14
58 3.2 Particle size distributions 15
59 3.2.1 Task 1 – Analysis of strontianite colloidal stability 15
60 3.2.2 Task 2 – Analysis of calcite colloidal stability 18
61 3.2.2.1 Effect of brine composition and concentration on particle concentration estimation for
62 $CaCO_3$ 19
63 3.2.3 Conclusions from PSD analysis for Task 1 20
64 3.2.4 Conclusions from particle concentration analysis for Task 2 21
65 4 Recommendations to improve data quality and expand colloids work 21
66 4.1 Updated TP 22
67 4.2 Experimental changes 22
68 4.2.1 Measuring particle size distributions and concentrations 24
69 4.2.2 Measuring zeta potential 24
70 4.2.3 Steady-state equilibrium behavior and population balance modeling 25
71 4.2.4 Inorganic colloid interaction with other waste components 26
72 4.2.5 Actinide sorption to colloids 27
73 4.3 Effect of direct brine releases on colloid transport 28
74 5 Acknowledgements 28
75 6 References 28
76 7 Appendix A: Plots of starting particle size distributions 33

Information Only

8 Appendix B: Plots of batch experimental data 34
9 Appendix C: Initial calcite settling kinetics 45

Information Only

List of Figures

Figure 1: Time-trend of strontianite (Test #2) concentration during the first hour of settling in 100X diluted ERDA-6 brine. The solid line represents a non-linear regression and the dashed lines represent the 95% confidence interval. 12
Figure 2: Strontianite particle size distributions after experiment termination (dry milled, Test #1). Light brown circles are individual data points and dark brown circles are mean values. Error bars represent one standard deviation from the mean (n = 4). Note: in some cases, there is a great deal of spread to the data and the error bars extend below zero to give a negative particle size, which is physically meaningless and not displayed. Compare to Table 13 in Kirkes (2020). Starting particle distributions are shown in Figure A-1. 16
Figure 3: Strontianite particle size distributions after experiment termination (wet milled, Test #2). Light red circles are individual data points and dark red circles are mean values. Error bars represent one standard deviation from the mean (n = 4). Note: in some cases, there is a great deal of spread to the data and the error bars extend below zero to give a negative particle size, which is physically meaningless and not displayed. Compare to Table 18 in Kirkes, 2020. Starting particle distributions are shown in Figure A-2. 17
Figure A-1: Zoomed in plot of Figure 1. Dashed horizontal lines are the starting distribution percentiles (numbers on the right axis) from Table 13 in Kirkes (2020). 33
Figure A-2: Zoomed in plot of Figure 2. Dashed horizontal lines are the starting distribution percentiles (numbers on the right axis) from Table 18 in Kirkes (2020). 33
Figure B-1: Elemental calcium concentration over experiment duration (top) and over 1 hr (bottom) for calcite in GWB (top). The dashed lines indicate the "baseline" ranging from 10.59 to 10.63 mM Ca (duplicate measurements). 34
Figure B-2: Elemental calcium concentration over experiment duration (top) and over 1 hr (bottom) for calcite in ERDA-6. The dashed lines indicate the "baseline" ranging from 9.36 to 9.43 mM Ca (duplicate measurements). 35
Figure B-3: Elemental calcium concentration over experiment duration (top) and over 1 hr (bottom) for calcite in 0.1 m NaCl. The dashed lines indicate the "baseline" ranging from 0.140 to 0.142 mM Ca (duplicate measurements). 36
Figure B-4: Elemental strontium concentration over experiment duration (top) and over 1 hr (bottom) for strontianite in GWB (Test #1). The dashed lines indicate the "baseline" ranging from 0.6306 to 0.6364 mM Sr (duplicate measurements). Note that there is minimal change in concentration from the initial time point at 0.02 hour (1 minute) to the second to last sampling point at 1 hour within the scatter of the data. 37
Figure B-5: Elemental strontium concentration over experiment duration (top) and over 1 hr (bottom) for strontianite in ERDA-6 (Test #1). The dashed lines indicate the "baseline" ranging from 0.227 to 0.228 mM Sr (duplicate measurements). Note that there is minimal change in concentration from the initial time point at 0.02 hour (1 minute) to the second to last sampling point at 1 hour within the scatter of the data. 38
Figure B-6: Elemental strontium concentration over experiment duration (top) and over 1 hr (bottom) for strontianite in 100X diluted ERDA-6 (Test #1). The dashed lines indicate the "baseline" ranging from 0.1856 to 0.1902 mM Sr (duplicate measurements). 39
Figure B-7: Elemental strontium concentration over experiment duration (top) and over 1 hr (bottom) for strontianite in 0.1 m NaCl (Test #1). The dashed lines indicate the "baseline" ranging from 0.2074 to 0.2086 mM Sr (duplicate measurements). Note that after a slight decrease from the 0.02 hr (1 minute) mark, there is minimal change in concentration up to the second to last sampling point at 1 hour within the scatter of the data. The decrease from 0.02 to 0.08 (5 minutes) hours could indicate

Information Only

rapid settling of the larger (i.e., greater than colloid size) particles in the system or that the initial concentration of 0.7849 mM in reactor 8-1 is a potentially anomalous measurement. 40
Figure B-8: Elemental strontium concentration over experiment duration (top) and over 2 hr (bottom) for strontianite in GWB (Test #2). The dashed lines indicate the "baseline" ranging from 0.6306 to 0.6364 mM Sr (duplicate measurements). 41
Figure B-9: Elemental strontium concentration over experiment duration (top) and over 2 hr (bottom) for strontianite in ERDA-6 (Test #2). The dashed lines indicate the "baseline" ranging from 0.227 to 0.228 mM Sr (duplicate measurements). 42
Figure B-10: Elemental strontium concentration over experiment duration (top) and over 1 hr (bottom)for strontianite in 100X diluted ERDA-6 (Test #2). The dashed lines indicate the "baseline" ranging from 0.1856 to 0.1902 mM Sr (duplicate measurements). Note the change in concentration between 1 hr and 72 hr appears negligible....43
Figure B-11: Elemental strontium concentration over experiment duration (top) and over 1 hr (bottom) for strontianite in 0.1 m NaCl (Test #2). The dashed lines indicate the "baseline" ranging from 0.2074 to 0.2086 mM Sr (duplicate measurements). 44
Figure C-1: Evaluating initial kinetics of calcite particle settling in GWB (left) and ERDA-6 (right). Solid lines represent linear regressions and dashed lines represent 95% confidence intervals. Note: different y-axes. 45

Information Only

List of Tables

Table 1: CCCs reported in literature for geogenic colloids 11
Table 2: Estimated remaining particle size after gravitational settling 14
Table 3: Average, standard deviation, and relative standard deviation of duplicate (n = 2) Mastersizer runs to assess repeatability* 18
Table C-1: Initial kinetics of particle settling 45

Information Only

Acronyms and Abbreviations

AP	Analysis Plan
AR	Analysis Report
Ca	Calcium (elemental)
CCA	Compliance Certification Application
CCC	Critical coagulation concentration
CI	Confidence interval
CO_2	Carbon dioxide
CO_3^{2-}	Carbonate
CRA	Compliance Recertification Application
C_T	Total [dissolved] inorganic carbon concentration
DBRs	Direct Brine Releases
DLS	Dynamic light scattering
DLVO	Derjaguin, Landau, Verwey, and Overbeek
DOE	Department of Energy
Dv(10)	Particle size in microns below which 10% of the sample lies
Dv(50)	Particle size in microns at which 50% of the sample is smaller and 50% is larger. Also known as the mass median diameter or the median of the volume distribution
Dv(90)	Particle size in microns below which 90% of the sample lies
EDL	Electrical double layer
EDTA	Etheylenediaminetetraacetic acid
EPA	Environmental Protection Agency
ERDA-6	Energy Research and Development Administration well 6 (synthetic Castile Formation brine)
ERMS	Electronic Record Management System
FTIR	Fourier transform infrared spectroscopy
FY	Fiscal year
GWB	Generic Weep Brine (synthetic Salado Formation brine)
ICP-AES	Inductively Coupled Plasma Atomic Emission Spectroscopy
m	Molal (i.e., moles solute per kilogram solvent)
M	Molar (i.e., moles per liter)
MgO	Magnesium oxide
mL	Milliliter
mm	Millimeter
mM	Millimolar
nm	Nanometer
NOM	Natural organic matter
PA	Performance assessment
PC	Particle concentration
PDI	Potential determining ions
pH	Negative logarithm of hydrogen ion activity
ppm	Parts per million
PSD	Particle size distribution
QA	Quality Assurance
RSD	Relative standard deviation

Information Only

SD	Standard deviation
SGWB	Simplified Generic Weep Brine
SN	Scientific notebook
SNL	Sandia National Laboratories
SP	Activity/Project Specific Procedures
Sr	Strontium (elemental)
TP	Test Plan
µm	Micrometer
UV-vis	Ultraviolet visible spectroscopy
W	Stability ratio
WIPP	Waste Isolation Pilot Plant
10X	Ten times
100X	One hundred times
$\bar{x}$	Average
[ ]	Concentration
>	Greater than
%	Percent

157

Information Only

158 # 1 *Introduction*

159 This report documents data analysis of the batch settling results presented in the
160 milestone report (Kirkes, 2020) for two carbonate mineral fragment colloids – calcite ($CaCO_3$)
161 and strontianite ($SrCO_3$). The methods herein follow the data analysis approach of AP-187 Rev.
162 0 (Hora et al., 2021) to analyze particle size distributions after experiment termination and total
163 metal concentrations in acidified samples with dissolved and particulate constituents. The
164 objective of this report is to evaluate the experimental plan and data from TP 14-04 Rev. 3
165 (Kirkes et al., 2018), completing data analysis for Tasks 1 and 2 from AP-187. The outcomes of
166 the data analysis are recommendations for future analyses that include new experimental
167 approaches such as zeta potential measurement, nano size particle distribution analysis, and
168 actinide adsorption calculations and studies. New analysis approaches and methods will improve
169 the colloid parameters used in WIPP PA calculations (DOE, 2019; Appendix PA). Colloid
170 formation is an important component of the PA because colloids can increase actinide mobilities.
171 New experimental designs and recommendations for updating the SNL WIPP colloids analysis in
172 Section 4 of this report will be applied to develop methods for MgO colloids experiments (Task
173 3a in Section 5 of AP-187), and the optimized methods will subsequently be implemented for
174 magnesite and brucite (Tasks 3b and 3c, respectively).

175 The WIPP PA conceptual models consider the existence of four types of colloids:
176 intrinsic, humic, mineral fragment, and microbial colloids (DOE, 2019; Appendix PA). Mineral
177 fragment colloids can also encompass lead/iron corrosion products and mineral-organic products.
178 In this report, we discuss the mineral fragments colloids: strontianite (Task 1) and calcite (Task
179 2).

180 # 2 *Methods for analysis of stability experiments*

181 This report documents steps to analyze time resolved concentration data and particle size
182 distribution data (in the spreadsheets associated with the milestone report: "SrCO3 test.xlsx" and
183 "CaCO3 test.xlsx") for strontianite and calcite batch settling experiments. Files associated with
184 this analysis are located at: cvs/CVSLIB/WIPP_EXTERNAL/AP187.

Information Only

2.1 Aggregation kinetics

2.1.1 Time resolved concentration data

Dissolved and colloidal metal concentrations (i.e., Ca or Sr in ppm) collected from mineral fragment instability experiments were measured over time from 1 minute to 2-3 days at room temperature under ambient laboratory conditions. Average concentrations presented in Kirkes (2020) were converted to molar units and data was re-plotted to show duplicates; figures for strontianite and calcite in GWB, ERDA-6, 100X diluted ERDA-6, and 0.1 m NaCl brines are shown in Appendix B. Typically, kinetic analysis was limited to 1 or 2 hours based on visual inspection of the data to perform fitting for rate constants; later values tended to overlap and not vary substantially (>10%) within the scatter of the measured data points. Initial analyses were focused on the results from the highest and lowest nominal ionic strength conditions (i.e., GWB with an ionic strength of ~8.3 m and 100X diluted ERDA-6 with an ionic strength of ~0.06 m) to discern whether a difference in aggregation rate could be seen at different brine salinities. The kinetic analysis was stopped when the 1 minute to 1 hour results did not vary, given insufficient data after the 1 hour mark to calculate kinetics rates within any sort of proper experimental resolution.

2.1.1.1 Data fitting

Regressions were performed in Minitab® (version 20.1.3). Linear or non-linear regressions were used to fit the data points and derive phenomenological aggregation/settling rates based on the relationship between concentration of instable mineral fragment species and time. The applied regression equations were compared to common kinetics rate laws to help interpret results.

2.2 Particle size distributions and particle concentration/number

Kirkes (2020) reported averaged standard percentile volume distribution, Dv(10), Dv(50), and Dv(90), results outputted from the Malvern Mastersizer 3000® particle size analyzer (Tables 13 and 18 of the milestone report). This report presents the mean values and descriptive statistics. Standard deviations for the four averaged values are calculated in Minitab® (version 20.1.3). Additional descriptive statistics (mean, standard deviation, and relative standard deviation) are calculated and presented for duplicate analyses of a single sample to assess repeatability. Displaying measurement and/or experimental error allows for a broader discussion of data quality.

Information Only

3 *Results and conclusions*

3.1 Estimate of particle settling kinetics

In theory mineral fragment colloids present in a quiescent repository long-term would quickly agglomerate due to the collapse of the repulsive energy barrier to colloid interaction at high ionic strengths. This has been known for decades since early work now referred to universally as DLVO theory. Papenguth and Behl (1996) demonstrated this empirically for the WIPP system and their experiments confirmed that brines are effective at promoting aggregation of mineral colloids, showing that the mobile actinide source term associated with mineral colloids is relatively small.

Table 1 shows CCCs for mineral or natural colloids from literature. The CCC is the estimated ionic strength (or salt concentration) at which mineral fragment colloids gravimetrically settle, where colloid agglomeration becomes diffusion limited and electrostatic repulsion negligible (Czigany et al., 2005; Einarson and Berg, 1993; Elimelech et al., 1998; Ross and Morrison, 1988).

Table 1: CCCs reported in literature for geogenic colloids

Colloid type	CCCs	Electrolyte composition	Reference
Clay	Up to 150 mM	Monovalent cations such as Na^+ and K^+	van Olphen (1991)
	0.5 – 2 mM	PDI like Mg^{2+}, Ca^{2+}, SO_4^{2-}, and CO_3^{2-} (Ding et al., 2018)	
Bentonite clay	1 mM	$CaCl_2$ solutions	Seher et al. (2007)
Plutonium	100 mM	1:1 electrolyte solution at pH 11.4	Abdel-Fattah, et al. (2013)
Natural sediments	90 – 200 mM	Pure Na electrolyte solutions	Czigany et al. (2005)
	1.7 – 3.6 mM	Pure Ca electrolyte solutions	

The WIPP system is unique among nuclear waste repositories in that both the near-field and far-field environments contain high ionic strength groundwaters. The primary WIPP brines are GWB with an estimated ionic strength of 8.25 m and ERDA-6 with an estimated ionic strength of 5.86 m (Xiong, 2008), which are tens of times greater than the literature CCCs for mineral or natural colloids reported above. This means that WIPP conditions should favor mineral colloid aggregation and a low mobile actinide source term.

Information Only

Because WIPP brines are quite concentrated and aggregation/coagulation would be expected to occur quickly for destabilized particles, a subset of the short-term stability data presented in the milestone report was analyzed and included here after an initial review of experimental design, data quality, and application to PA. Colloid research during the CCA demonstrated this phenomena (Papenguth and Behl, 1996), and repeating CCA experiments does not add tremendous value beyond reaffirming common knowledge.

3.1.1 Task 1 – Analysis of strontianite colloidal stability

Particle settling rate constants were determined by fitting concentration versus time data. Figure 1 is a sample fitting for the lowest ionic strength brine solution studied – 100X diluted ERDA-6 should have a nominal ionic strength of around 0.06 m.

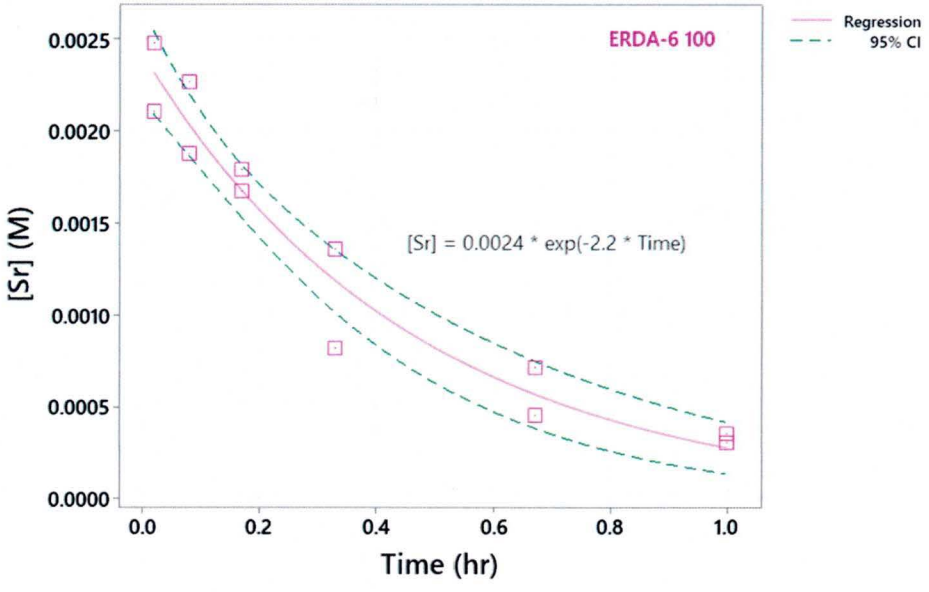

Figure 1: Time-trend of strontianite (Test #2) concentration during the first hour of settling in 100X diluted ERDA-6 brine. The solid line represents a non-linear regression and the dashed lines represent the 95% confidence interval.

The estimated settling rate constant for wet milled strontianite in 100X diluted ERDA-6 is 2.2 ± 0.6 hr^{-1}, which predicts that the strontium concentration decreases by half in 0.3 hours or almost 19 minutes. The change in particle concentration over time was proportional to the instantaneous particle concentration as represented by equation 1:

$$\frac{dN}{dt} \propto N \quad (1)$$

Information Only

where N is the particle concentration and t is time. The rapid particle settling rate is thus a function of the particle concentration. The derived kinetics are the result of the experiments consisting of concentrated dispersions and the high particle loading influencing settling behavior. Being able to accurately quantify particle concentrations throughout the time course of the experiment would have allowed for improved understanding of how the population number or concentration of particles changed as a function of certain experimental conditions.

3.1.2 Task 2 – Analysis of calcite colloidal stability

Similar to strontianite, particle settling rate constants were determined by fitting concentration versus time data. Preliminary fits and results for calcite in NaCl, ERDA-6, SGWB, and GWB are presented in Appendix C.

3.1.3 Estimating settling times and average particle size for Tasks 1 and 2

Stokes Law (equation 2; Benjamin and Lawler, 2013), which describes gravitional settling of larger particles, can be used to roughly estimate the average particle size at the time of experiment termination. Conversely, estimating settling time presuming sedimination is the predominant removal mechanism (due to a high percentage of particles at least 1 μm in size) gives a sense of when the larger particles might be completely settled in the batch systems.

$$v = \frac{(\rho_p - \rho_L) g d_p^2}{18\mu} \quad (2)$$

where v is Stokes' velocity (m-s^{-1}), ρ_p is the particle density (kg-m^{-3}), ρ_L is the liquid or fluid density (kg-m^{-3}), g is the gravitational constant (m-s^{-2}), d_p is the particle diameter (m), and μ is the fluid viscosity (kg-m^{-1}-s^{-1}). Assumptions made to apply Stokes Law include: spherical particles and low Reynolds number (neglecting inertial terms), ρ_p = 2.71 g-cm^{-3} for calcite and ρ_p = 3.78 g-cm^{-3} for strontianite, ρ_L = 1.193 g-cm^{-3} for a saturated NaCl solution, and μ = 0.001676 kg-m^{-1}-s^{-1} for a NaCl solution with that density. A height of 100 mm was selected based on an expected depth in the settling experiments from visual inspection of photographs included in the milestone report (Kirkes, 2020). This is an approximation because the height of the solution column was not reported nor were test tube dimensions provided to be able to generate an estimate based on volume of solution dispensed (ranging from 20 to 30 mL) irrespective of the displacement from addition of ground mineral mass (ranging from 10 – 100 mg). Experiments were terminated after 96 hours for calcite experiments and either 48 or 72 hours for strontianite.

Information Only

Error! Reference source not found. presents the estimated average remaining particle size from simplified assumptions of the experimental system. At termination of the experiments, it is possible that particles smaller than ~0.8 μm (in particular, those ≤ 0.2 μm) might still have been present and suspended in solution. However, as an additional caveat to this estimation, agglomeration and settling were most likely occurring at the same time in the polydisperse, concentrated experimental solutions.

Table 2: Estimated remaining particle size after gravitational settling

Mineral	Settling time (hr)	Particle size (μm)
Calcite	48	1.1
	96	0.8
Strontianite	48	0.8
	72	0.7

It would take an estimated 56 hours for 1 μm calcite particles and 33 hours for 1 μm strontianite particles to completely gravitationally settle out under the conditions mentioned above. Excluding time resolved concentration measurements collected earlier than those times would focus the analysis on submicron particles and their settling behavior.

3.1.4 Conclusions from settling rates for Tasks 1 and 2

The preliminary comparisons of short-term aggregation data in this report confirm previous understanding from the CCA and literature; aggregation and settling were concurrently occurring within the first 1 or 2 hours for most experiments. The recent experiments (Kirkes, 2020) consisted of concentrated polydisperse mineral suspensions containing a great deal of larger particles (i.e., >1 μm and thus outside the colloidal size range), which also influences aggregation kinetics because there are correlations between particle concentration and particle diameter with rate of collisions and settling speed.

Based on the preliminary estimation using Stokes Law, there is a distinct possibility that the aggregation and settling behavior of the macro-sized particles was captured in the experiments while colloid behavior was not adequately captured. While the total element concentration returns to a so-called baseline at the end of many of the experiments, it cannot be determined from the collected data whether the baseline is purely dissolved concentrations of the element. Therefore, it must be acknowledged that the "baseline" could be a combination of

Information Only

dissolved and particulate metal concentrations in the acidified sample. This also means that parsing particle aggregation and settling kinetics from the concentration data is more challenging since it is predicated on using the measured metal concentration as a proxy for particle concentration. Section 3.2.2.1 continues the discussion on particle concentration calculations, focusing on calcite.

Collecting more datapoints at more frequent time invervals and reducing scatter and measurement variability (in particular, through implementation of more sensitive techniques) in future experiments will allow us to draw statistically meaningful conclusions. Not only is improved experimental resolution needed to detect settling of very small particles, more work must be done to characterize analyte-specific instrumental limits of detection and quantification to assess whether the measurement technique has sufficient sensitivity. Additional experimental methods are considered in the recommendations provided in Section 4.

3.2 Particle size distributions

Particle size distributions were collected for strontianite and calcite before and after settling experiments. The data was treated as described in the milestone report (Kirkes, 2020) – "The results include the averages of 2 runs for each sample and then also the average of the two duplicate samples. (i.e. GWB SrCO3 is the Average of: GWB SrCO3 1-1 run 1, GWB SrCO3 1-1 run 2, GWB SrCO3 1-2 run 1 and GWB SrCO3 1-2 run 2)" – to determine the mean values. The only differences are that the mean values and the error from averaging of the data points are visualized and displayed in the figures below.

3.2.1 Task 1 – Analysis of strontianite colloidal stability

Figure 2 shows the mean Dv(10), Dv(50), and Dv(90) values and the associated standard deviations for dry milled strontianite after termination of settling experiments.

Information Only

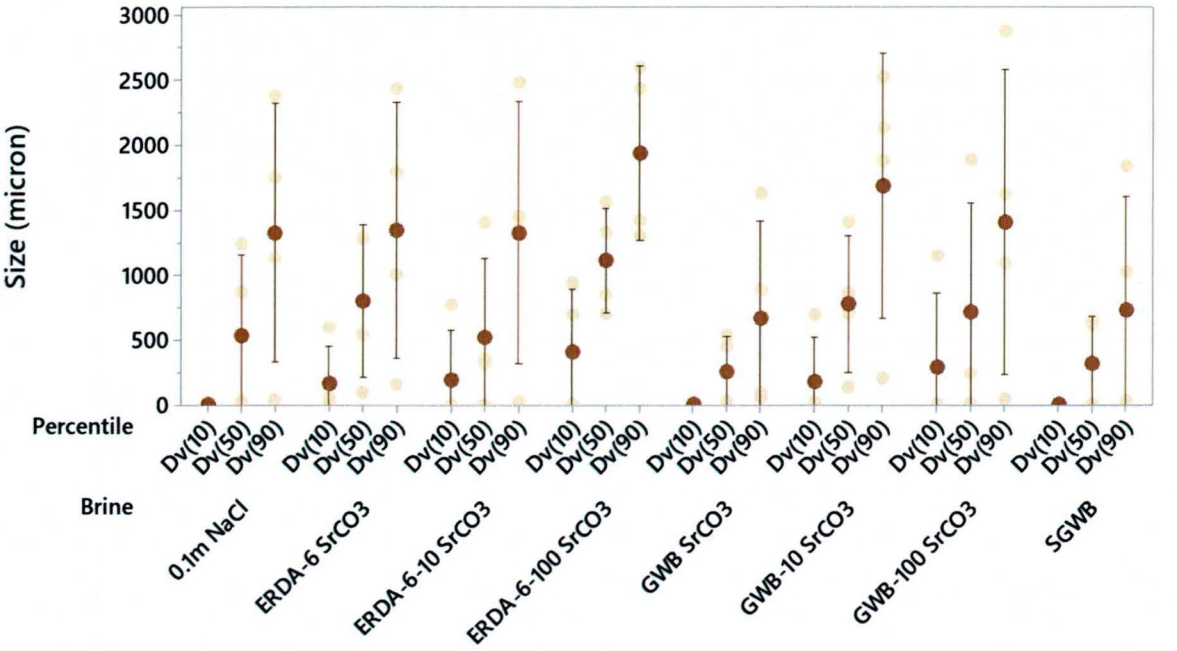

Figure 2: Strontianite particle size distributions after experiment termination (dry milled, Test #1). Light brown circles are individual data points and dark brown circles are mean values. Error bars represent one standard deviation from the mean (n = 4). Note: in some cases, there is a great deal of spread to the data and the error bars extend below zero to give a negative particle size, which is physically meaningless and not displayed. Compare to Table 13 in Kirkes (2020). Starting particle distributions are shown in Figure A-1.

Figure 3 shows the mean Dv(10), Dv(50), and Dv(90) values and the associated standard deviations for wet milled strontianite after termination of settling experiments.

Information Only

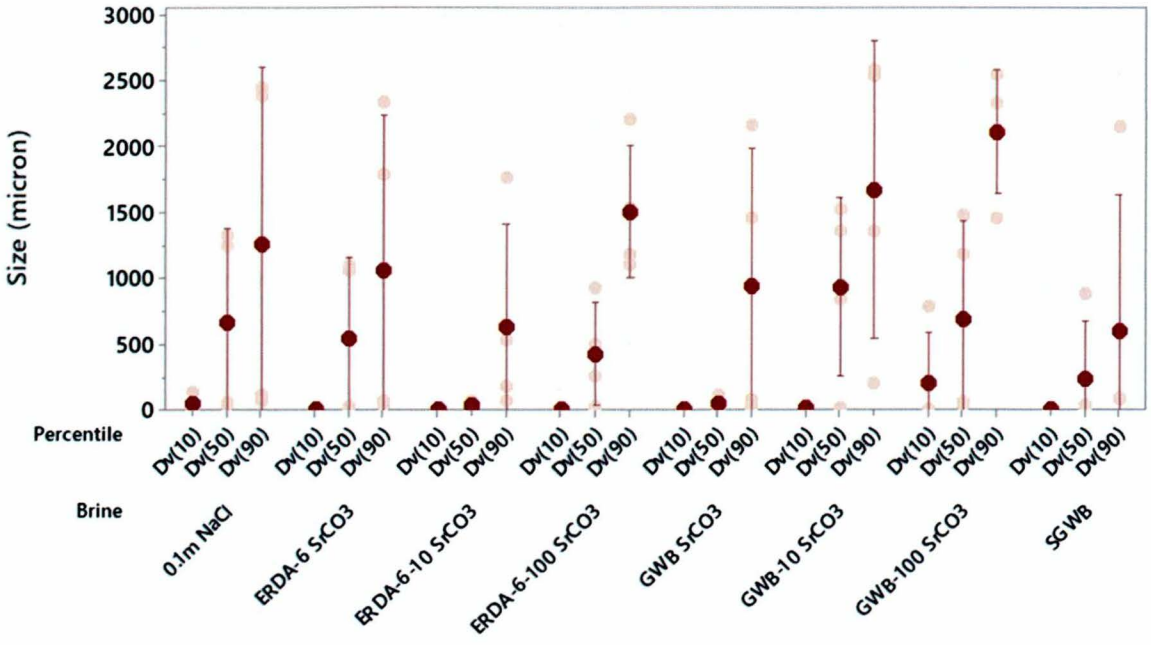

Figure 3: Strontianite particle size distributions after experiment termination (wet milled, Test #2). Light red circles are individual data points and dark red circles are mean values. Error bars represent one standard deviation from the mean (n = 4). Note: in some cases, there is a great deal of spread to the data and the error bars extend below zero to give a negative particle size, which is physically meaningless and not displayed. Compare to Table 18 in Kirkes, 2020. Starting particle distributions are shown in Figure A-2.

Strontianite instability experiments employing strontianite particles ground using the dry milling process (i.e. without a solvent; designated $SrCO_3$ Test #1) were terminated on 6/25/2019 based on the entry in SN WIPP-Colloids-3 page 36. The remaining solutions and solid in the test tubes were kept for particle size analysis at a future date per the SN and the milestone report (Kirkes, 2020). Particle size analysis was initiated on 8/9/2019 for the first set of reactors (i.e., 1-1, 2-1, etc.) and each reactor sample was analyzed twice on the instrument (i.e., reactor 1-1 was analyzed in duplicate with the second measurement occurring after the first measurement was completed). Samples from the duplicate reactors (i.e., 1-2, 2-2, etc.) were analyzed 27 days later on 9/5/2019 (SN WIPP-Colloids-3 page 64).

The Mastersizer software applies a scattering model, such as Mie theory, to calculate size distributions from the measured scatter pattern. The measured and predicted scattering data are overlain and compared and the goodness of the data fit is quantified as the Residual or Weighted Residual, which are displayed in the measurement analysis report (Malvern Panalytical, 2020).

Information Only

The milestone report (Kirkes, 2020) states in section 2.2: "The Residual, is an indication on how well the analysis data was fitted to the measurement data. A good fit is indicated by a residual of under 1%." Typically, the residual and weighted residual should be similar. Many of the measurements have weighted residuals >1%, (see SN WIPP-Colloids-3 page 64 and SN WIPP-Colloids-3 page 65).

Comparing duplicate runs for the same sample (Table 3), large standard deviations are observed; relative standard deviations greater than 3, 5, 6, or 10%[1] are highlighted in Table 3.

Table 3: Average, standard deviation, and relative standard deviation of duplicate (n = 2) Mastersizer runs to assess repeatability*

Test #1	$\bar{x}$ (µm)	SD	RSD (%)	$\bar{x}$ (µm)	SD	RSD (%)	$\bar{x}$ (µm)	SD	RSD (%)
Sample ID	Dv(10)			Dv(50)			Dv(90)		
GWB SrCO3 1-1	1.35	1.44	106.21	268.70	376.61	140.16	465.8	587.18	126.06
GWB-10 SrCO3 2-1	348.30	490.31	140.77	1135.00	388.91	34.27	2325	275.77	11.86
GWB-100 SrCO3 3-1	1.49	0.08	5.69	478.00	335.17	70.12	1355	374.77	27.66
ERDA-6 SrCO3 4-1	33.50	36.35	108.53	909.50	523.97	57.61	1395	558.61	40.04
ERDA-6-10 SrCO3 5-1	0.64	0.01	2.11	341.50	28.99	8.49	1400	70.71	5.05
ERDA-6-100 SrCO3 6-1	1.31	0.65	50.10	776.00	103.24	13.30	1360	84.85	6.24
SGWB 7-1	2.23	2.35	105.72	633.50	20.51	3.24	1430	579.83	40.55
0.1m NaCl 8-1	2.05	1.31	63.97	1055.00	261.63	24.80	2065	445.48	21.57
Test #2	$\bar{x}$ (µm)	SD	RSD (%)	$\bar{x}$ (µm)	SD	RSD (%)	$\bar{x}$ (µm)	SD	RSD (%)
Sample ID	Dv(10)			Dv(50)			Dv(90)		
GWB SrCO3 1-1	0.29	0.04	15.23	16.99	21.66	127.52	745.15	1010.95	135.67
GWB-10 SrCO3 2-1	4.45	5.83	130.96	686.00	953.18	138.95	1366.5	1645.44	120.41
GWB-100 SrCO3 3-1	394.73	554.76	140.54	1330.00	212.13	15.95	2435	148.49	6.10
ERDA-6 SrCO3 4-1	7.08	9.64	136.07	531.34	747.64	140.71	915.55	1236.66	135.07
ERDA-6-10 SrCO3 5-1	0.37	0.08	20.42	17.51	16.53	94.42	1146.5	867.62	75.68
ERDA-6-100 SrCO3 6-1	1.15	0.94	82.04	263.15	336.37	127.82	1320	296.98	22.50
SGWB 7-1	0.36	0.11	30.71	445.51	627.19	140.78	1117.35	1460.39	130.70
0.1m NaCl 8-1	66.87	93.52	139.85	689.80	891.24	129.20	1283	1650.39	128.64

* Data shown for the first set of reactors (i.e., Z-1 where $1 \leq Z \leq 8$). Duplicate measurements of each replicate reactor (i.e., reactor series Z-2) exhibit similarly high error.

3.2.2 Task 2 – Analysis of calcite colloidal stability

Particle size analysis was performed for calcite on 9/25/2019 after the batch settling experiments were terminated; the method for strontianite (i.e., particle refractive index for

[1]Based on ISO 13320 related to the response of laser diffraction instruments for particle sizes ranging from approximately 0.1 µm to 3.0 mm, the coefficient of variation (also known as relative standard deviation) should be < 3% for d50 and < 5% for d10 and d90; doubled values (6% and 10%, respectively) are valid for particles smaller than 10 µm (Kuchenbecker et al., 2012).

Information Only

strontianite) was used to analyze final distributions and thus the calcite data was discarded on 11/18/2019 (SN WIPP-Colloids-3 page 65).

3.2.2.1 Effect of brine composition and concentration on particle concentration estimation for $CaCO_3$

An alternative way to estimate particle concentration (described in Section 3.2.2. of AP-187) is to use the time-resolved concentration data (i.e., $[Me]_{total}$; see Appendix B for plots of that data) and the so-called baseline elemental concentrations (i.e., $[Me]_{matrix}$; equation 5 in AP-187) in the brines. However, there are challenges to back calculating particle concentration from total concentration of acidified colloidal dispersions alone, some of which are outlined below.

Brines were "equilibrated" with the respective mineral solids (e.g., calcite) and then filtered with a 0.2 μm filter prior to being used in experiments (Kirkes, 2020). The measured element concentration (i.e., Ca) after the equlibration period was designated a "baseline" initial concentration in the brines. Because particles <0.2 μm would still been in solution after filtration, the baseline concentration cannot be presumed to be just dissolved Ca. Additionally, the brines already contain Ca (GWB has 13.8 mM of Ca^{2+} and ERDA-6 has 12.0 mM of Ca^{2+} per SP 20-4 Appendix B; Xiong, 2008). Ca baselines for experiments in GWB and ERDA-6 measured by ICP-AES (Figure B-3 and Figure B-4) are lower than the brine Ca concentrations, suggesting precipitation of Ca-contaning solids, which could be colloidal, during brine equilibration with calcite. The acidified total Ca concentration via ICP measures both dissolved and particulate Ca in the system. But because both brines contain Ca to begin with, estimates cannot be made of calcite equilibration purely from measured Ca. Un-acidified Ca (no nitric acid addition) needs to be known to proceed. For accuracy, the total dissolved concentration of calcium is needed in order to evaluate the particulate concentration via the AP procedure.

Furthermore, this approach requires understanding of mineral solubility; dissolved concentrations can be estimated if equilibria (log Ks) are established. In the 100X diluted brines, increased Ca is observed (e.g., 0.259 mM versus 0.138 mM Ca for calcite equilibrated in diluted GWB and 0.472 mM versus 0.120 mM for calcite equilibrated in diluted ERDA-6). The greater Ca concentration in the brine could be indicative of calcite dissolution during the equilibration period, but the measurements do not verify whether the brines were sufficiently saturated to prevent further dissolution of ground calcite particles and/or oversaturation of Ca before the stability experiments. It is difficult to estimate C_T (dissolved and particulate) and thus the

Information Only

409 solubility of $CaCO_3$(s) for several reasons: inorganic carbon was not directly measured; there
410 was the possibility (albiet slim) for CO_2 partitioning at various points during the experiment,
411 which was conducted on the bench top under ambient laboratory conditions, where solutions
412 were left open to the atmosphere during repeated sampling; and because pH was only measured
413 once for the "equilibrated" brine just after the equilibration step. This means that thermodynamic
414 modeling with EQ3/6 cannot be relied on to calculate solubilites or saturation indices.

415 ***3.2.3 Conclusions from PSD analysis for Task 1***

416 The causes of the errors observed in the $SrCO_3$ PSD measurements are unknown. The
417 lapse of months between experiment termination and particle size analysis could have
418 contributed to the broad particle size distribution measurements as seen in Figures 2 and 3.
419 Because the samples were kept outside the glovebox, there might have been CO_2 intrusion,
420 however unlikely, into the samples affecting the chemistry. Moreover, agglomeration could have
421 occurred during sample storage. Samples could have also been agitated during handling and
422 sampling. Residue contamination in the sample dispersion unit from previously analyzed
423 samples is another possibility.

424 Results of duplicate runs suggest that during the analysis itself another factor affected
425 measurement repeatability. It is possible that aggregation and disaggregation of particles
426 simultaneously occurred in the samples, which were sonicated in the Malvern Mastersizer
427 sample dispersion unit during the particle size measurements; or, that the concentration of larger
428 particles in the polydisperse suspension biased the results. Perhaps the sample optical density is
429 too high or too low or analysis method parameters needed to be adjusted to optimize the
430 measurements.

431 For future experiments a more robust, systematic approach in the data collection will be
432 prescribed in revised SPs and the TP in order to apply the analyses in AP-187. This will involve:
433 adhering to a shorter sampling schedule to mitigate settling occurring in between particle
434 analysis; determining sampling and analysis techniques that will reduce the potential for sample
435 agitation prior to or during sampling and analysis; implementing more detailed experimental
436 tasking and procedures to include methods, verification checklists for prescriptive actions like
437 cleaning, review of measurement quality control outputs (i.e., residual and other indicators of
438 goodness of fit generated by the Malvern software), and data validation steps incorporating

Information Only

uncertainty quantification. In addition, analyzing suspended (i.e., in sampled supernatant) particle sizes throughout batch experiments will provide more insight into colloid interactions so that the dynamics of particle populations can be characterized.

3.2.4 Conclusions from particle concentration analysis for Task 2

Checking the ranges of particles removed by different filtration techniques and filter types (pore size, material, etc.) is an ongoing effort within colloids work. Future experiments employing filtration will establish this information, especially when dealing with very small colloids (<0.2 μm), and determine associated uncertainty.

Verified solubility calculations are necessary to: validate the assumption of brine saturation before performing the settling experiments, evaluate equilibration times, and estimate dissolved elemental concentrations. Appropriate literature data will be used, if available, otherwise calculations will be performed using measurements of experimental constituents (e.g., for future experiments involving carbonate minerals carried out under ambient conditions, C_T will be measured in order to calculate equilibria).

Clearly quantifying particulate versus dissolved concentrations allows for the use of metal ion measurements to approximate particle number in experiments following AP-187. However, the challenges discussed in Section 3.2.2.1 demonstrate a need to refine the experimental approach and pursue using insoluble minerals or synthesis.

4 *Recommendations to improve data quality and expand colloids work*

This section includes modifications to experimental approaches and methods impacting data quality. The short-term stability experiments in Kirkes (2020) that used concentrated polydisperse suspensions with large particles to assess "presence" or "absence" of colloids and determinations of relatively fast aggregation kinetics give little predictive power. Expanded colloid work will validate or update the CONCMIN parameters and address EPA completeness questions related to mineral fragment colloids, such as MgO colloid formation. It will also advance the WIPP program's scientific understanding of colloidal behavior, interactions, and potential transport in the respository. Experiments will contribute to the broader WIPP program by ensuring data is useful for PA in advance of CRAs. Future work efforts, time, and resources will focus on enhancing the understanding of the underlying science using advanced analytical capabilities to emphasize addressing WIPP project priorities. Ultimately, the considerations presented below will inform a revision to TP 14-04 or a new TP commencing in FY 2022.

Information Only

4.1 Updated TP

Colloid instability experiments, which were performed for screening purposes during the CCA and proposed to be repeated in TP 14-04, provide some insight into the short-term behavior of colloidal particles in brines (Papenguth and Behl, 1996). However, phenomena occuring on the order of days or weeks (e.g., coagulation or aggregation kinetics and large particle settling) are but a blip on the post-closure 10,000 year timeframe. There is a need instead to better understand steady-state behavior of colloids, in particular small colloids, in the repository under quiescent conditions as well as the transient behavior of these colloids in the event of a perturbance, such as a drilling intrusion or other direct brine release scenario considered and modeled in PA.

A revision of TP 14-04 or creation of a new TP will consolidate SNL WIPP colloidal work into a single, cohesive TP and research program. The revised or new TP will broaden the definition of mineral fragment colloids to encompass possible mineral colloids formed due to corrosion and magnesium oxide hydration/carbonation

4.2 Experimental changes

For future experiments, the selection of colloids to be investigated or re-evaluated in order to update parameters will be targeted and strategic. The current version of TP 14-04 was proposed to investigate a wide array of mineral fragment colloids – most, if not all, already considered in the investigations performed during the CCA. At the conclusion of their experiments, Papenguth and Behl (1996) showed that hematite, goethite, and bentonite colloids were stabile, including in diluted simulated brine. Understanding and learning from these prior results can give us starting points for additional experiments and suggest that clays and/or iron mineral colloid stability should be examined more closely. More recent research has suggested that clay colloids can exhibit behavior counter to classic DLVO theory in higher ionic strength solutions (Missana and Adell, 2000).

Colloid stability is only one factor though. Minerals that sorb actinides will be prioritized, for example aluminosilicates over strontianite, depending on their presence in the waste inventory, repository horizon, and/or their generation by corrosion or oil and gas drilling.

Investigating mixtures of minerals (inorganics and clays) and minerals in the presence of organic ligands and acids also means that certain inorganic minerals that may not exhibit a particularly strong affinity for actinides alone are reassessed based on these more complex

Information Only

interactions. Experimental design is iterative; there is immense value starting with simplified experiments, though they may not be the most descriptive and representative of reality, and adding complexity. Intentionally configuring experiments in this manner can provide an understanding of specific phenomena as well as contribute to developing and parameterizing models of behavior, whether it be kinetics and/or mechanisms of reactions. Experiments can begin with monodisperse suspensions of well-characterized spherical particles with smooth surfaces and progress to evaluating bimodal and then heterodisperse populations if need be.

Other aspects to inform experimental design are: using insoluble minerals and using synthesis to generate small colloidal particles. The most recent experiments in TP 14-04 attempted to employ the fundamental approach of using the elemental concentration of acidified colloidal dispersions, compensating for the dissolved concentration ("baseline") present in the starting solutions, as a surrogate for the colloid population in the system – this was referred to as the PC in the AP. Because the two minerals being studied were somewhat soluble, there was a concern colloids would dissolve in the brines upon addition thus minerals were pre-dissolved in the brine. However, using elemental concentration as a proxy for particle concentration has shortcomings. In general, using insoluble model inorganic or mineral colloids would preempt and avoid unnecessary complications in data generation, analysis, and interpretation and allow for improved quantification of colloid particle populations. Possible candiates are: silica, silver, titanium dioxide, iron, and alumina among others. Analogues should be good matches for natural mineral properties like density, zeta potentials, etc. if they are considered.

If well-defined and characterized colloidal particles cannot be purchased, synthesis techniques (Matijevic, 1993; Park et al., 2001) should be pursued – if feasible and possible – to generate desired small mineral colloid particles; milling should not. Milling of mineral solids has variable results in terms of particle shapes and sizes. Crushing or grinding of solids to produce very fine powders could induce mineral surface and morphological changes that are not representatitive of in-situ processes that would lead to colloid generation. If milling will continue to be used, there must be more systematic study to understand how the different techniques (dry versus wet using ethanol as a solvent) affect the particles generated and whether heat generated from the friction of the milling process can impact the eventual particle composition. Additionally, for wet-milling, presence of residual solvent after milling and steps to wash or rinse particles to remove the solvent would need to be explored. That being said, mechanical

Information Only

532 milling has many limitations in producing colloidal size particles, in particular in the size range
533 that is of interest and relevant to the project. This can be seen from sizing information presented
534 in the milestone report (Kirkes, 2020), though that data must be regarded as qualitative given the
535 discussions on data quality presented previously in this report.

536 ***4.2.1 Measuring particle size distributions and concentrations***

537 Because small colloidal particles have been under studied in a WIPP-context, future work
538 will focus on characterizing their behavior in brines and their potential to transport actinides. The
539 Malvern Mastersizer 3000, the current instrument available to obtain PSDs, uses laser diffraction
540 and application of Mie theory to measure and estimate particle sizes ranging from 0.01 to 3500
541 µm per the manufacturer. The operational definition of colloids used for WIPP colloids work is
542 particles with one dimension ranging from 0.001 to 1 µm; therefore, the lowest threshold of the
543 Mastersizer is 10X greater than the smallest particle sizes of interest. The newly acquired
544 Malvern Zetasizer Nano employs light scattering to analyze even smaller particles (0.0003 to 10
545 µm); smaller colloidal particles in the nanoscale range could be of more concern from a transport
546 perspective and warrant further study. DLS in combination with UV-vis spectroscopy will allow
547 for improved characterization of particle size distributions, the hydrodynamic radius of particles,
548 and concentrations such that particle numbers can be back calculated and compared.
549 Additionally, the WIPP geochemistry group will establish collaborations with Sandia colleagues
550 to compare DLS with other techniques like laser induced dielectric breakdown detection.

551 ***4.2.2 Measuring zeta potential***

552 Analyzing the zeta potential of mineral fragment and other inorganic and organic colloids
553 at different pH values and ionic strength conditions gives valuable information about both
554 actinide uptake by colloids and actinide transport by colloids. This allows for characterization of
555 the electrical potential at the double layer and contributes to the overall understanding of particle
556 suspension stability in brines. Relationships can be derived between the Debye length and
557 salinity, and electric charge density is a key parameter for modeling colloid behavior following
558 DLVO theory. Using the Brookhaven Instruments NanoBrook ZetaPALS, zeta potential will be
559 evaluated with the salinity gradient and pH gradient, which is valuable to determining surface
560 absorption as well as particle aggregation under WIPP conditions.

Information Only

4.2.3 Steady-state equilibrium behavior and population balance modeling

To better understand the behavior of colloids in a quiescent system, the post-closure steady-state population of colloids after aggregation and settling must be quantified. This will entail more detailed and careful analysis of end-state results in experiments, including a comprehensive review of experimental and analytical uncertainties. Limits of detection and other metrics of analytical sensitivity should be well established, especially when conducting experiments dealing with smaller particles to ensure data quality as measurements approach lower detection or quantification limits of some analytical instruments. For example, in prior work involving sequential filtration using molecular weight cut off filters of decreasing pore size (i.e., MgO colloids experiments presented in Xiong, 2017), it was unclear whether no colloids within a certain size range (smaller than about 3 nm) were actually present in the filtrate or rather colloids of a certain size were merely no longer detectable or quantifiable within the experimental and analytical uncertainty. Additional validation steps such as performing electron microscopy on the filter surfaces or using spectroscopy will aid in confirming conclusions.

One way to constrain steady-state colloid stabilities is using the Smoluchowski equation (Benjamin and Lawler, 2013; Jeldres et al., 2018) and performing population balance modeling. The Smoluchowski equation presents a population balance for flocculating (or coagulating) particles in a suspension. It describes how the number concentration or population of each size particle in a discrete distribution changes over time. The equation can account for various flocculation mechanisms like differential sedimentation, Brownian motion, and shear. Terms accounting for floc breakup can be added. This work will be applied to better understanding the genesis of colloidal particles from precipitation and ensuing flocculation. Theoretical modeling is beneficial to complement experimental work or even provide insight that was missed from experimental results. However, certain judgements have to be made about variables such as collision frequency function and the function accounting for short-range transport forces and particle-particle interaction that perhaps cannot be informed by experimental data at hand. Numerical solutions to the Smoluchowski equation, some of which utilize open source Python code, can be found (e.g., Degueldre et al., 2009; Keck and Bortz, 2013; Mocz, 2017) and should be investigated further.

Another analytical approach promising to the WIPP is modelling flocculation with fractal dimensions given that flocs do not actually coalesce into spheres with a combined and conserved

Information Only

volume as is assumed by the Smoluchowski equation (Benjamin and Lawler, 2013; Jeldres et al., 2018). When flocs form from smaller particles, there can be void spaces present. This could have implications for sorption, capture of dissolved or colloidal actinides, and transport. Alternatively, molecular simulation could reveal detailed interactions between colloid particles at various conditions (e.g., concentration), with or without organic ligands, and resulting sorption of actinides.

Investigating natural processes and field conditions by collecting groundwater samples from monitoring wells within or near the WIPP land withdrawal boundry, measuring indigenous colloid concentrations, and characterizing the types of colloids detected deepens our understanding of the local geology and geochemistry. A combination of field measurements and experimental results could be complemented by published data on particle size distributions of colloids in natural waters (Filella and Buffle, 1993) and establish the potential for using natural analogs to describe phenomena in the WIPP post-closure.

4.2.4 Inorganic colloid interaction with other waste components

Prior WIPP investigations of inorganic colloids focused on behavior in simplified systems of respective mineral particles – in some cases concentrated dispersions – in representative synthetic brine solutions. More realistically, the repository environment will be a multicomponent system where inorganic colloids can coexist with organic ligands like EDTA and organic acids from soil or degrading cellulose, plastic, and rubber in the waste containers. The existence of these will be explored in the TP. NOM and fractions of NOM like humic and fulvic acids can coat and stabilize inorganic colloids dependent on pH, ionic strength, and concentration of PDIs (i.e., Ca^{2+}, Mg^{2+}, CO_3^{2-}, and SO_4^{2-}) (Mylon et al., 2004). NOM can contain quinone moieties, which are redox active functional groups (Uchimiya and Stone, 2009). Employing small molecular weight model quinone compounds, in addition to humic and fulvic acids, could be relevant to probe potential oxidation/reduction (redox) reactions in the presence of reduced NOM in an anoxic respository (Menezes et al., 2021; Tratnyek et al., 2012) for actinides potentially sorbing to NOM-coated mineral fragment colloids.

NOM is also known to chelate dissolved metal ions (Sonke and Salters, 2006; Stern et al., 2014; Tipping et al., 2002). Investigating competition of dissolved iron (Fujisawa et al., 2011) with actinides for sorption to colloids – similar to and combined with ongoing work on iron and EDTA – could be important given the high iron inventory in the repository. It could also be a

Information Only

623 tool for evaluating the conservatism associated with current humic and inorganic colloid sorption
624 models.
625 Furthermore, plastics present in the waste can breakdown into micro, or even nano, sized
626 particles due to synergistic mechanisms such as biodegradation, hydrolysis, and/or reaction with
627 radical species produced by radiolysis; microplastics are already known to be co-contaminants
628 that can sorb and transport heavy metals in marine, terrestrial, and subsurface environments
629 (Alimi et al., 2018). Small plastic particles can interact with other organic and inorganic colloids
630 present in the repository and could potentially serve as additional vectors for radionuclide
631 transport, warranting further study.
632 These mixed colloids can be analyzed with UV-vis and FTIR, new analytical methods
633 which will be included in the revision of TP 14-04.

634 ***4.2.5 Actinide sorption to colloids***
635 Prior determinations of actinide sorption to colloids, in particular very small colloids, will
636 be updated. The transport of actinides is related to their association with the enormous surface
637 area provided by a large number of minute particles (Swartz et al., 1997), which can be described
638 as the mobile surface area because it is the surface area of the suspended particles available for
639 actinide adsorption. While stability is important because aggregation can reduce accessible
640 surface area (Steefel and Van Cappellen, 1990; Strehlau et al., 2017), assumptions about the
641 stability of particles in WIPP brines should not preclude us from considering and studying
642 sorption and/or desorption. Developing mineral-specific isotherms, perhaps using chemical
643 analogs for the actinides, would refine sorption site density calculations and thereby decrease the
644 number of assumptions made in the CCA.
645 Interactions between NOM and Fe/Pb-containing minerals (Voelker and Sulzberger,
646 1996; Voelker et al., 1997) should be examined more closely becase they can induce changes in
647 the oxidation state of redox-sensitive actinides like Pu, U, and Np (Maher et al., 2013; Schmeide
648 and Bernhard, 2009). Formation, reactivity, and stability of these adsorbed complexes can be
649 evaluated using molecular modeling, which is a new capability within the SNL WIPP colloids
650 program.
651 The WIPP PA mineral fragment colloid contribution to the total actinide mobilization,
652 S_MIN, is modeled as S_MIN = CONCMIN (boundary value) (DOE, 2019; Appendix PA).
653 Additional investigation of actinide sorption to colloids is likely to identify a new parameter,

Information Only

654 such as a proportionality factor of actinde mineral fragment colloid to the dissolved actinide (for
655 example, PROPMIN) and upgrade the mineral fragment model to:

656 $$S\_MIN = min(CONCMIN, PROPMIN \times S\_DIS) \quad (3)$$

657 where S_DIS represents the dissolved contribution to the total mobilized concentration.

658 **4.3 Effect of direct brine releases on colloid transport**

659 Considerations of colloidal transport of actinides during a DBR – including potential
660 chemistry changes from such an intrusion into an inundated repository, characterizing the fluid
661 flow paths induced by an intrusion (fractured, channelized, etc.) – warrants further experimental
662 and/or modeling work beyond what was previously done for the CCA, especially since DBRs
663 were not a major driver for total releases back then (DOE, 1996; Chapter 6). Collaborations with
664 PA will be developed to enhance understanding of WIPP conceptual models and PA calculations
665 if there is a desire to explore colloid transport during a release scenario in greater depth.

666 DBRs, short duration releases of brine to the surface after borehole penetration of WIPP,
667 dominate total releases at low probabilties in the current baseline in CRA-2019 (Zeitler et al.,
668 2019). Because releases through Culebra Dolomite are orders of magnitude less than other
669 release mechanisms, DBR events are more of a focus in the PA than long-term releases through
670 the Culebra. The maximum cumulative flow rate over 10,000 years was 7,540 m^3 (or an average
671 volumetric flow rate of 0.75 m^3-$year^{-1}$) for releases through a borehole into the Culebra Dolomite
672 (Day, 2019). Whereas, modeling of non-zero DBR events gives substantially higher mean brine
673 releases of 15.02 m^3 over 3 to 4.5 days (or average flow rates between 3.3 and 5 m^3-day^{-1})
674 (Bethune, 2019). The maximum modeled release event gives a brine volume of 105.79 m^3, which
675 equates to an average flow rate of 23.5 m^3-day^{-1} (Bethune, 2019).

676 **5 *Acknowledgements***

677 The authors thank Hans Papenguth for valuable input to this work, Pat Brady for insightful
678 comments, and Seth King for information on DBRs.

679 **6 *References***

680 Abdel-Fattah, A.I., Zhou, D.X., Boukhalfa, H., Tarimala, S., Ware, S.D. and Keller, A.A. (2013)
681 Dispersion Stability and Electrokinetic Properties of Intrinsic Plutonium Colloids:
682 Implications for Subsurface Transport. Environ Sci Technol 47, 5626-5634.

Information Only

683 Alimi, O.S., Farner Budarz, J., Hernandez, L.M. and Tufenkji, N. (2018) Microplastics and
684 Nanoplastics in Aquatic Environments: Aggregation, Deposition, and Enhanced
685 Contaminant Transport. Environ Sci Technol 52, 1704-1724.

686 Benjamin, M.M. and Lawler, D.F. (2013) Water quality engineering: physical/chemical treatment
687 processes. John Wiley & Sons, Hoboken, N.J.

688 Bethune, J. (2019) Analysis Package for Direct Brine Release in the 2019 Compliance
689 Recertification Application Performance Assessment (CRA-2019 PA). Revision 0. Sandia
690 National Laboratories, Carlsbad, NM. ERMS #571370

691 Czigany, S., Flury, M. and Harsh, J.B. (2005) Colloid stability in vadose zone aggregate. Hanford
692 sediments. Environ Sci Technol 39, 1506-1512.

693 Day, B. (2019) Analysis Package for Salado Flow in the 2019 Compliance Recertification
694 Application Performance Assessment (CRA-2019 PA). Revision 0. Sandia National
695 Laboratories, Carlsbad, NM. ERMS #571368

696 Degueldre, C., Aeberhard, P., Kunze, P. and Bessho, K. (2009) Colloid generation/elimination
697 dynamic processes: Toward a pseudo-equilibrium? Colloid Surface A 337, 117-126.

698 Ding, H., and Rahman, S. R. (2018) Investigation of the impact of potential determining ions
699 from surface complexation modeling. Energy & Fuels, 32(9), 9314-9321.

700 DOE (1996) Title 40 CFR Part 191 Compliance Certification Application for the Waste Isolation
701 Pilot Plant. DOE/CAO-1996-2184. U.S. Department of Energy, Carlsbad, NM.

702 DOE (2019) Title 40 CFR Part 191 Subparts B and C Compliance Recertification Application
703 2019 for the Waste Isolation Pilot Plant. DOE/WIPP-19-3609, Rev. 0. U.S. Department of
704 Energy, Carlsbad, NM

705 Einarson, M.B. and Berg, J.C. (1993) Electrosteric Stabilization of Colloidal Latex Dispersions.
706 J Colloid Interf Sci 155, 165-172.

707 Elimelech, M., Jia, X., Gregory, J. and Williams, R. (1998) Particle Deposition and Aggregation:
708 Measurement, Modelling and Simulation. Elsevier Science & Technology, Oxford, United
709 States.

710 Filella, M. and Buffle, J. (1993) Factors Controlling the Stability of Submicron Colloids in
711 Natural-Waters. Colloid Surface A 73, 255-273.

712 Fujisawa, N., Furubayashi, K., Fukushima, M., Yamamoto, M., Komai, T., Ootsuka, K., and
713 Kawabe, Y. (2011) Evaluation of the iron(II)-binding abilities of humic acids by
714 complexometric titration using colorimetry with ortho-phenanthroline, Humic Substances
715 Research, v.8, 1-6.

716 Hora, P., Miller, C., Jang, J., Kirkes, L., and Zhang, L. (2021) AP-187 Revision 0: Analysis Plan
717 for the Experimental Investigation of Stability of Mineral Colloids Under WIPP
718 Conditions. Sandia National Laboratories, Carlsbad, NM. ERMS #575618

Information Only

719 Jeldres, R.I., Fawell, P.D. and Florio, B.J. (2018) Population balance modelling to describe the
720 particle aggregation process: A review. Powder Technol. 326, 190-207.

721 Keck, D.D. and Bortz, D.M. (2013) Numerical simulation of solutions and moments of the
722 smoluchowski coagulation equation. arXiv preprint arXiv:1312.7240.

723 Kirkes, L., Mariner, P., and Sisk-Scott, C. (2018) Experimental Investigation of Stability of
724 Mineral Colloids Under WIPP Conditions. TP 14-04 Rev. 3. Sandia National
725 Laboratories, Carlsbad, NM. ERMS #570240.

726 Kirkes, L. (2020) Fourth Milestone Report on Test Plan TP 14-04, Rev. 3. Experimental
727 Investigation of Stability of Mineral Colloids under WIPP Conditions. Sandia National
728 Laboratories, Carlsbad, NM. ERMS #574417

729 Kuchenbecker, P., Gemeinert, M. and Rabe, T. (2012) Inter-laboratory Study of Particle Size
730 Distribution Measurements by Laser Diffraction. Particle & Particle Systems
731 Characterization 29, 304-310.

732 Maher, K., Bargar, J.R. and Brown, G.E., Jr. (2013) Environmental speciation of actinides. Inorg
733 Chem 52, 3510-3532.

734 Malvern Panalytical Ltd. (2020) Mastersizer 3000 User Guide. MAN0474-09-EN-00, January
735 2020

736 Matijevic, E. (1993) Preparation and properties of uniform size colloids. Chem. Mat. 5, 412-426.

737 Menezes, O., Kadoya, W.M., Gavazza, S., Sierra-Alvarez, R., Mash, E.A., Abrell, L. and Field,
738 J.A. (2021) Covalent binding with model quinone compounds unveils the environmental
739 fate of the insensitive munitions reduced product 2,4-diaminoanisole (DAAN) under anoxic
740 conditions. J Hazard Mater 413, 10.

741 Minitab Statistical Software (2020) State College, PA: Minitab, Inc. (www.minitab.com)

742 Missana, T. and Adell, A. (2000) On the applicability of DLVO theory to the prediction of clay
743 colloids stability. J Colloid Interf Sci 230, 150-156.

744 Mocz, P. (2017) Smoluchowski Equations Solver. MIT, GitHub.

745 Mylon, S.E., Chen, K.L. and Elimelech, M. (2004) Influence of Natural Organic Matter and Ionic
746 Composition on the Kinetics and Structure of Hematite Colloid Aggregation: Implications
747 to Iron Depletion in Estuaries. Langmuir 20, 9000-9006.

748 Papenguth, H. W., and Behl, Y. K. (1996) Test plan for evaluation of colloid-facilitated actinide
749 transport at the Waste Isolation Pilot Plant. Sandia National Laboratories Waste Isolation
750 Pilot Plant Test Plan TP 96-01. ERMS 417319.

751 Park, J., Privman, V. and Matijevic, E. (2001) Model of formation of monodispersed colloids. J
752 Phys Chem B 105, 11630-11635.

Information Only

753 Ross, S. and Morrison, I.D. (1988) Colloidal Systems and Interfaces. Wiley-Interscience, New
754 York, pp. xvii + 422.

755 Schmeide, K. and Bernhard, G. (2009) Redox stability of neptunium(V) and neptunium(IV) in the
756 presence of humic substances of varying functionality. Radiochim Acta 97, 603-611.

757 Seher, H., Schaefer, T., Geckeis, H. and Fanghaenel, T. (2007) FEBEX bentonite colloid stability
758 in ground water, Sweden, pp. 397-402.

759 Sonke, J. E. and Salters, V. J. M. (2006) Lanthanide–humic substances complexation. I.
760 Experimental evidence for a lanthanide contraction effect. Geochimica et Cosmochimica
761 Acta, Volume 70, Issue 6, 1495-1506.

762 Steefel, C. I. and van Cappellen, P. (1990) A new kinetic approach to modeling water-rock
763 interaction: The role of nucleation, precursors, and Ostwald ripening. Geochimica et
764 Cosmochimica Acta 54, 2657-2677.

765 Stern, J. C., Foustoukos, D. I., Sonke, J. E., and Salters, V. J. M. (2014) Humic acid
766 complexation of Th, Hf and Zr in ligand competition experiments: Metal loading and pH
767 effects. Chemical Geology, 363, 241-249.

768 Strehlau, J.H., Toner, B.M., Arnold, W.A. and Penn, R.L. (2017) Accessible reactive surface area
769 and abiotic redox reactivity of iron oxyhydroxides in acidic brines. Geochim Cosmochim
770 Ac 197, 345-355.

771 Swartz, C. H., Ulery, A. L., and Gschwend, P. M. (1997) An AEM-TEM study of nanometer-
772 scale mineral associations in an aquifer sand: Implications for colloid mobilization.
773 Geochimica et Cosmochimica Acta 61, 707-718.

774 Tipping, E., Rey-Castro, C., Bryan, S. E., and Hamilton-Taylor, J. (2002) Al(III) and Fe(III)
775 binding by humic substances in freshwaters, and implications for trace metal speciation.
776 Geochimica et Cosmochimica Acta 66, 3211-3224.

777 Tratnyek, P.G., Grundl, T.J., Haderlein, S.B. and American Chemical Society, D.o.E.C.S. (2012)
778 Aquatic Redox Chemistry. American Chemical Society, Washington, DC, United States.

779 Uchimiya, M. and Stone, A.T. (2009) Reversible redox chemistry of quinones: Impact on
780 biogeochemical cycles. Chemosphere 77, 451-458.

781 van Olphen, H. (1991) An Introduction to Clay Colloid Chemistry: For Clay Technologists,
782 Geologists, and Soil Scientists. 2nd ed. Malabar, Fl: Krieger Pub. Co. (Reprint or 1977-2nd
783 edition originally published by John Wiley & Sons.)

784 Voelker, B. M. and Sulzberger, B. (1996) Effects of fulvic acid on Fe(II) oxidation by hydrogen
785 peroxide. Environmental Science and Technology 30(4), 1106-1114.

786 Voelker, B. M., Morel, F. M. M., and Sulzberger, B. (1997) Iron redox cycling in surface waters:
787 Effects of humic substances and light. Environmental Science and Technology 31(4),
788 1004-1011.

Information Only

789 Xiong, Y.-L. (2008) Preparing Synthetic Brines for Geochemical Experiments, SP 20-4,
790 Revision 2, Sandia National Laboratories, Carlsbad, New Mexico, U.S.A. ERMS
791 #549757.

792 Xiong, Y.-L. (2017) Absence of Mineral Colloids in High Ionic Strength Solutions Associated
793 with Salt Formations: Experimental Determination and Applications to Nuclear Waste
794 Management. Sandia National Laboratories, Carlsbad, NM. ERMS #568244

795 Zeitler, T., Bethune, J., Brunell, S., Kicker, D., and Long, J. (2019) Summary Report for the
796 2019 Compliance Recertification Application Performance Assessment (CRA-2019 PA).
797 Revision 0. Sandia National Laboratories, Carlsbad, NM. ERMS #571376

Information Only

7 *Appendix A: Plots of starting particle size distributions*

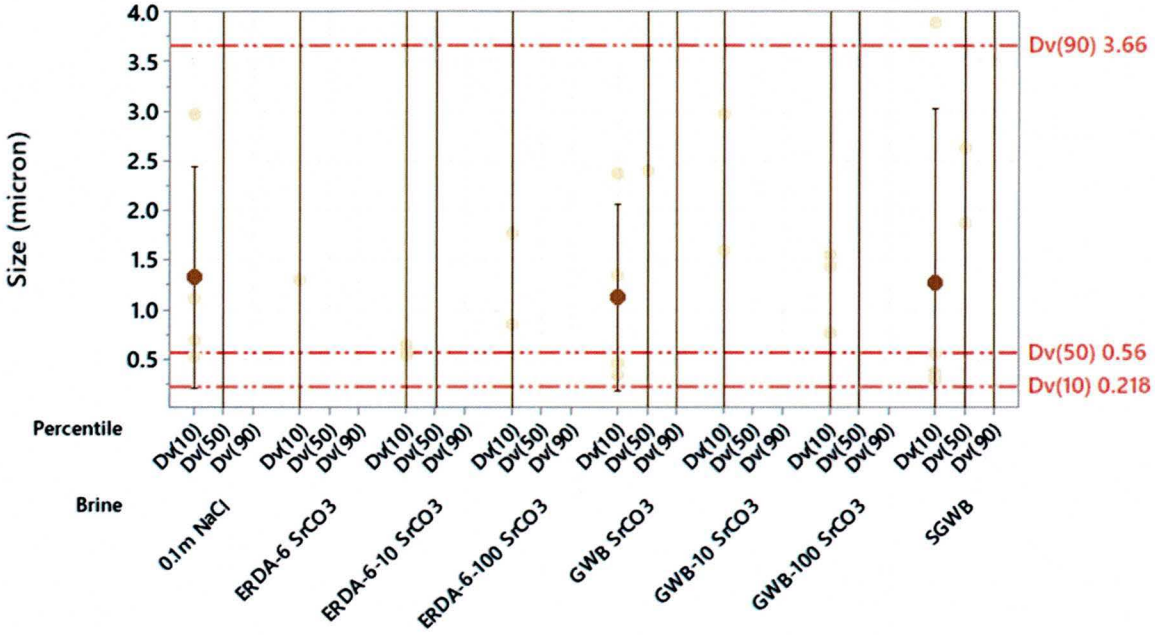

Figure A-1: Zoomed in plot of Figure 2. Dashed horizontal lines are the starting distribution percentiles (numbers on the right axis) from Table 13 in Kirkes (2020).

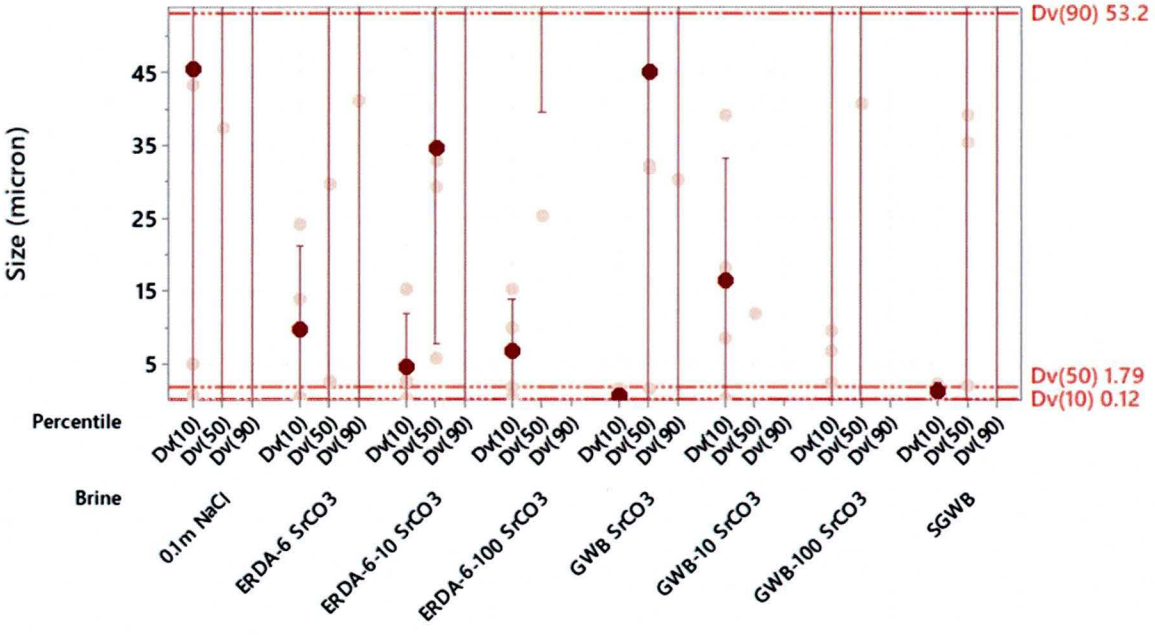

Figure A-2: Zoomed in plot of Figure 3. Dashed horizontal lines are the starting distribution percentiles (numbers on the right axis) from Table 18 in Kirkes (2020).

Information Only

8 *Appendix B: Plots of batch experimental data*

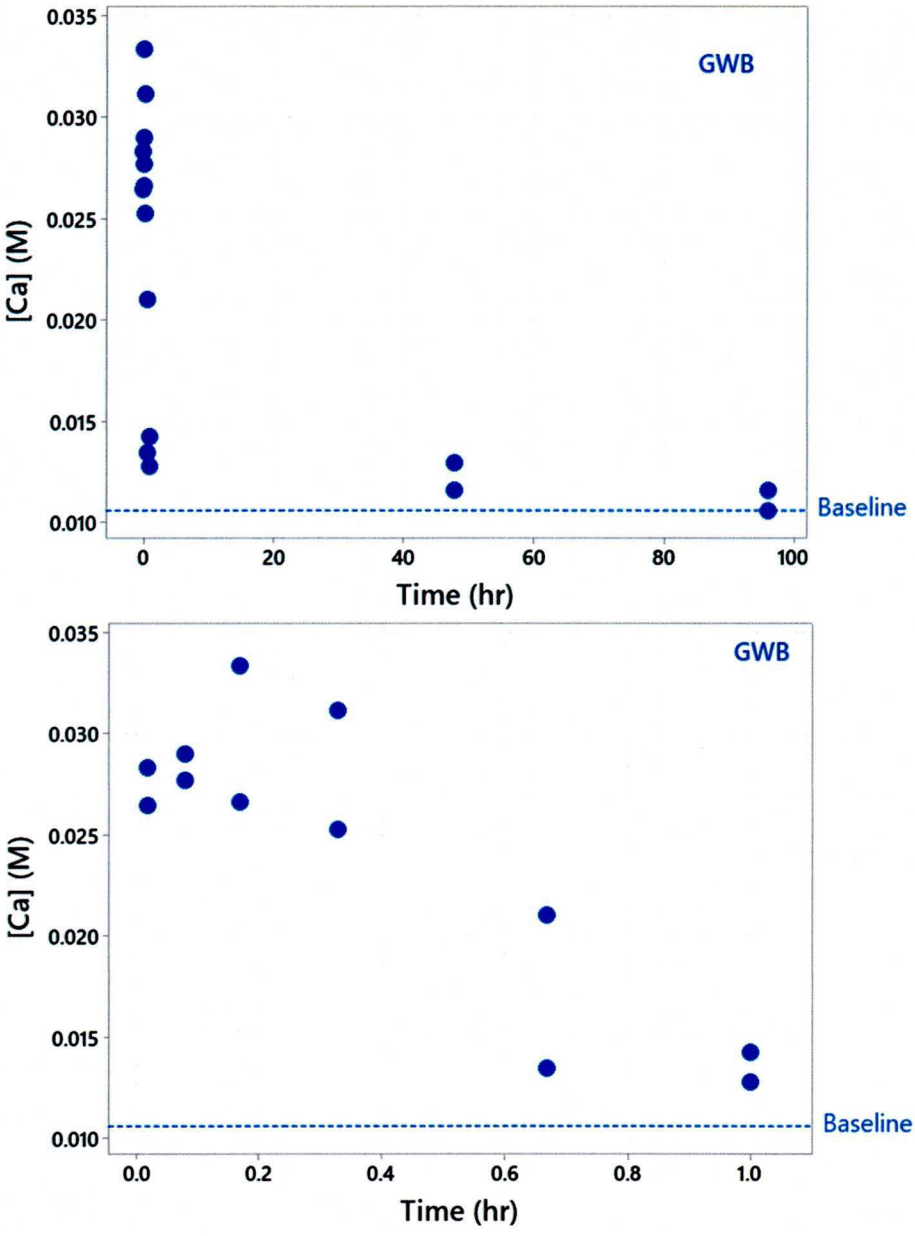

Figure B-3: Elemental calcium concentration over experiment duration (top) and over 1 hr (bottom) for calcite in GWB (top). The dashed lines indicate the "baseline" ranging from 10.59 to 10.63 mM Ca (duplicate measurements).

Information Only

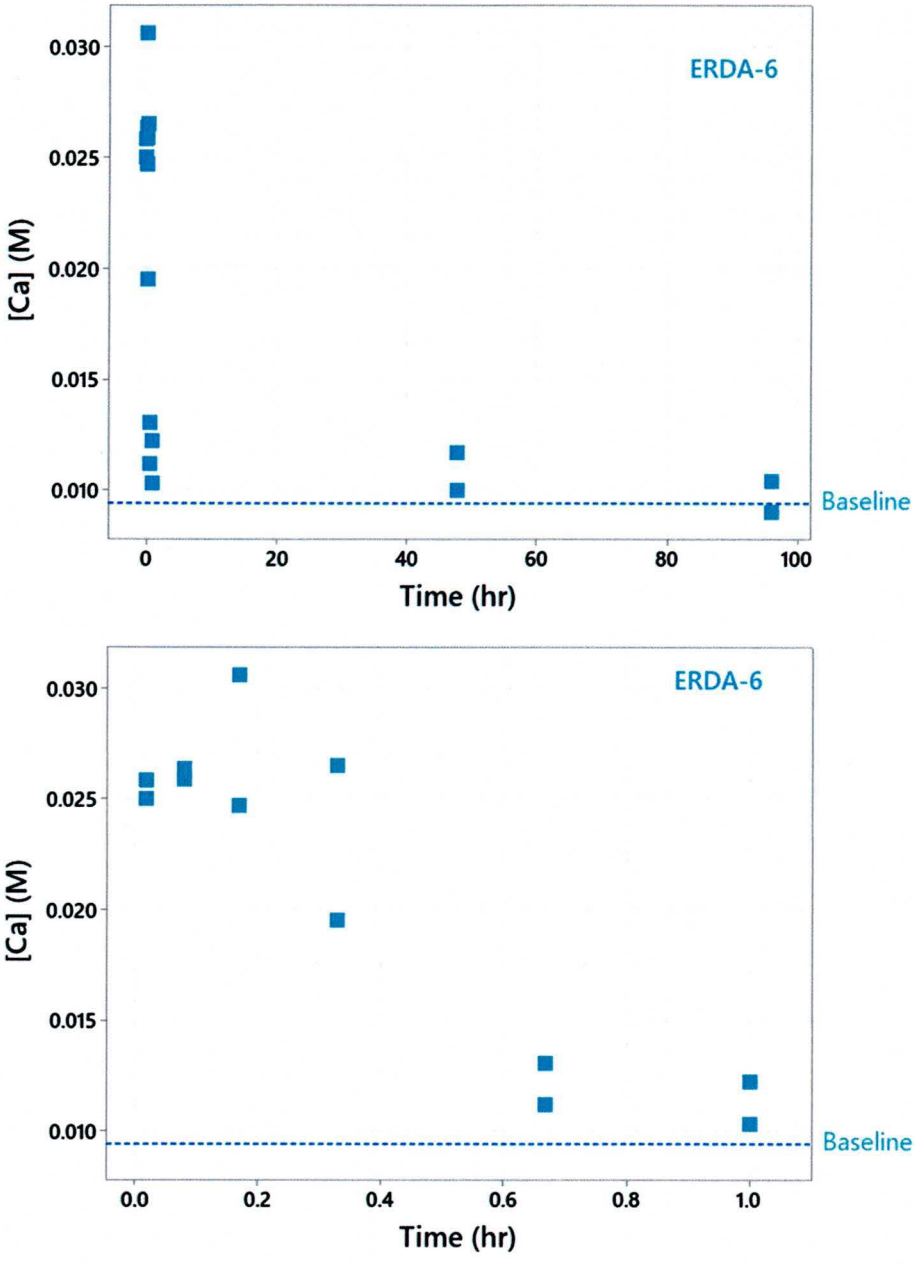

Figure B-4: Elemental calcium concentration over experiment duration (top) and over 1 hr (bottom) for calcite in ERDA-6. The dashed lines indicate the "baseline" ranging from 9.36 to 9.43 mM Ca (duplicate measurements).

Information Only

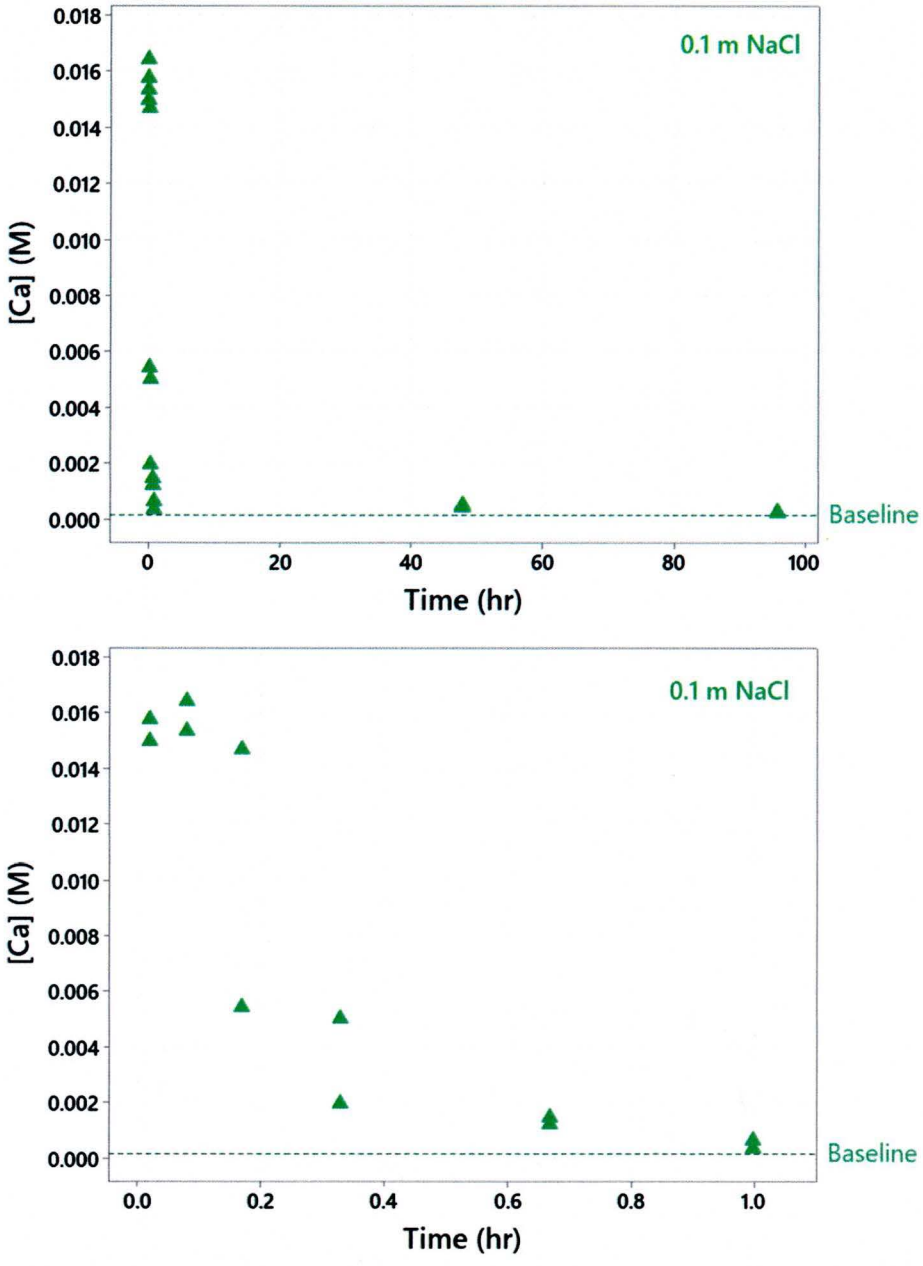

Figure B-5: Elemental calcium concentration over experiment duration (top) and over 1 hr (bottom) for calcite in 0.1 m NaCl. The dashed lines indicate the "baseline" ranging from 0.140 to 0.142 mM Ca (duplicate measurements).

Information Only

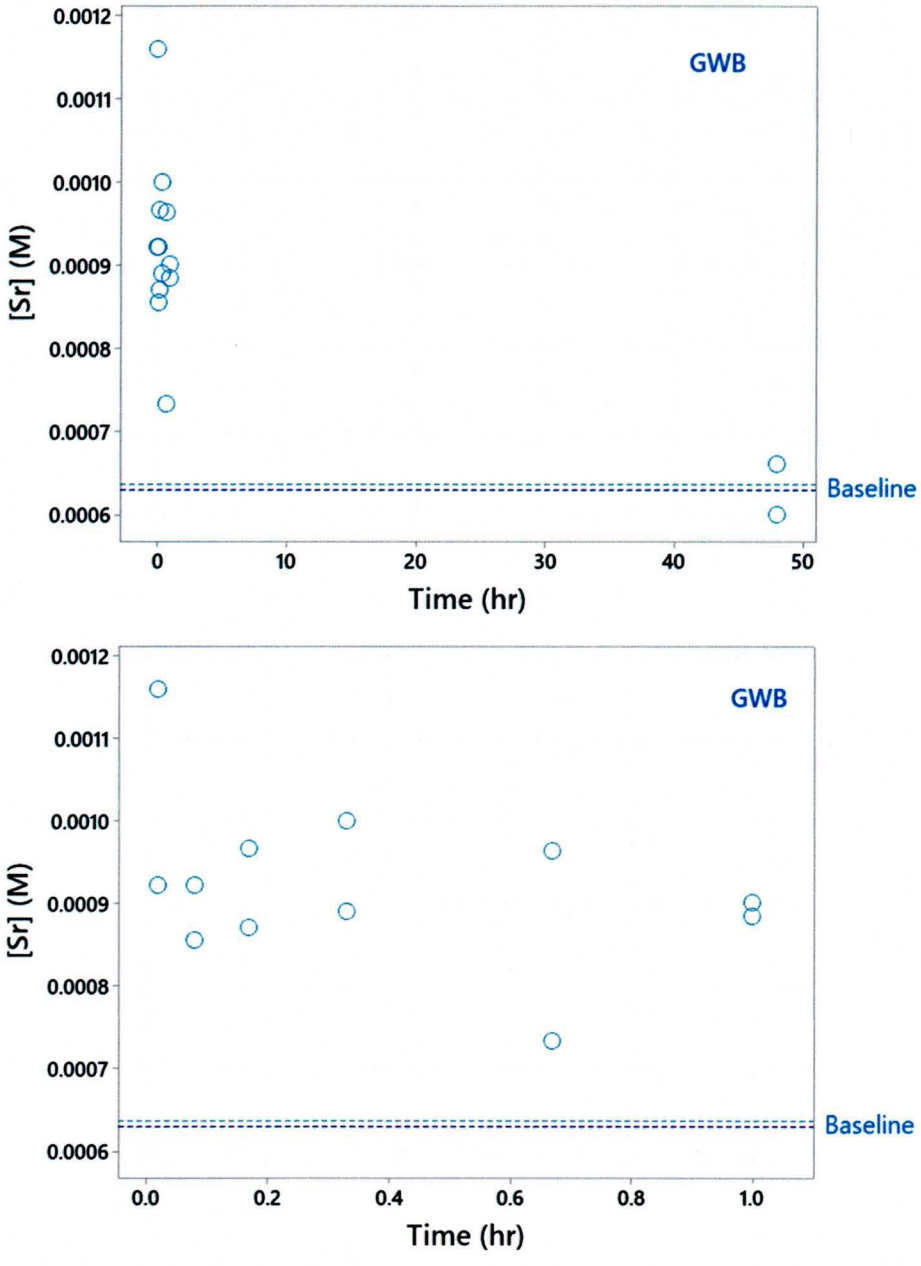

828

829

830 Figure B-6: Elemental strontium concentration over experiment duration (top) and over 1 hr (bottom) for
831 strontianite in GWB (Test #1). The dashed lines indicate the "baseline" ranging from 0.6306 to 0.6364
832 mM Sr (duplicate measurements). Note that there is minimal change in concentration from the initial time
833 point at 0.02 hour (1 minute) to the second to last sampling point at 1 hour within the scatter of the data.

834

Information Only

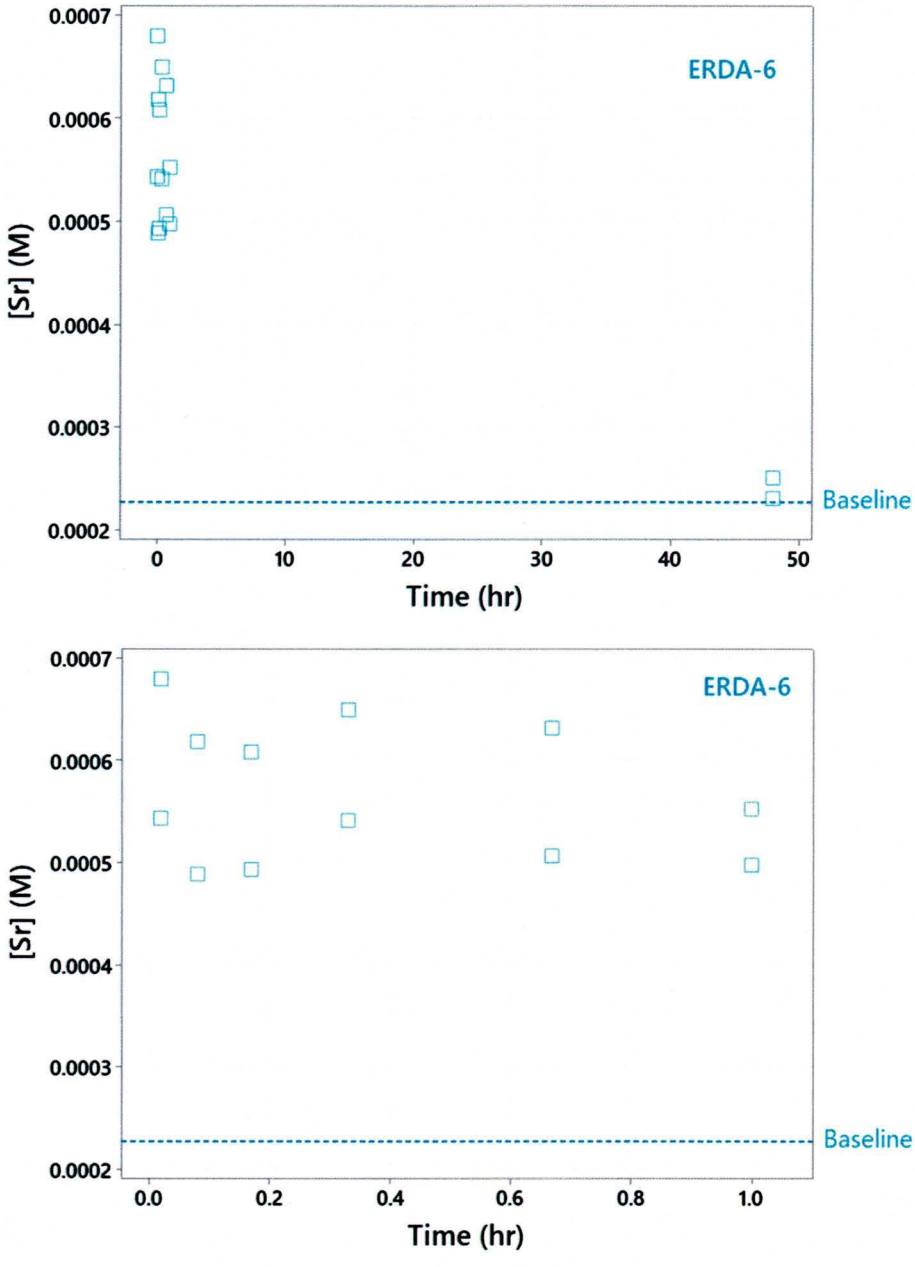

Figure B-7: Elemental strontium concentration over experiment duration (top) and over 1 hr (bottom) for strontianite in ERDA-6 (Test #1). The dashed lines indicate the "baseline" ranging from 0.227 to 0.228 mM Sr (duplicate measurements). Note that there is minimal change in concentration from the initial time point at 0.02 hour (1 minute) to the second to last sampling point at 1 hour within the scatter of the data.

Information Only

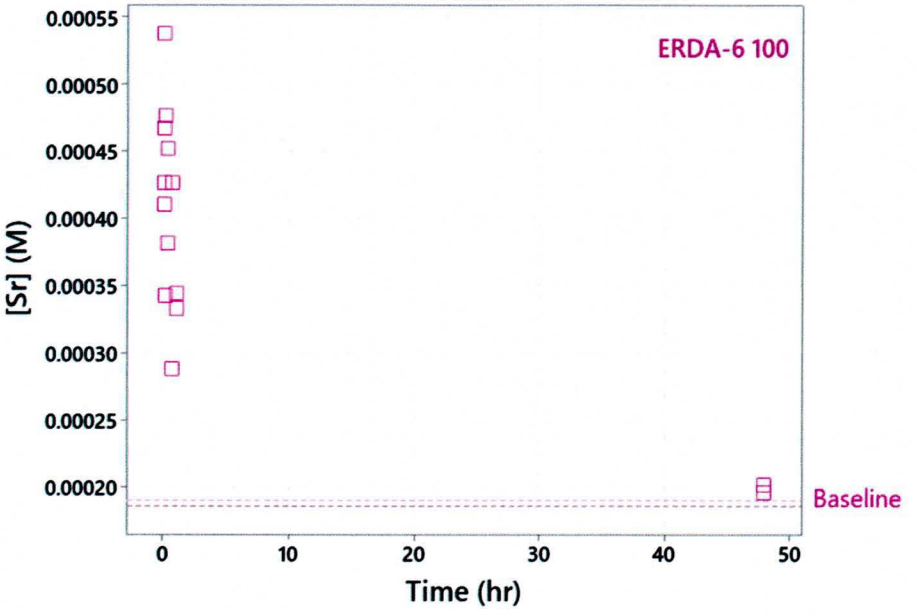

841

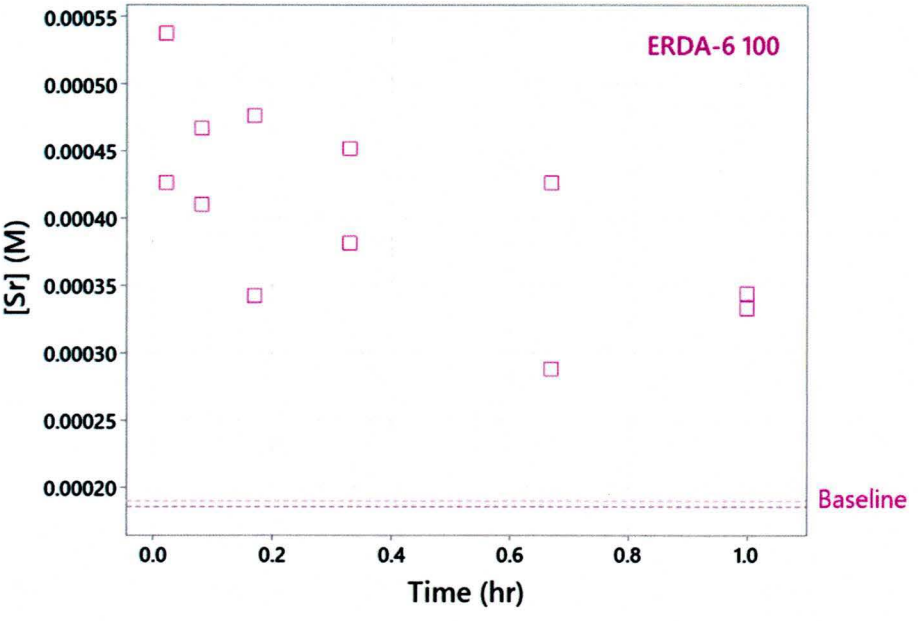

842

843 Figure B-8: Elemental strontium concentration over experiment duration (top) and over 1 hr (bottom) for
844 strontianite in 100X diluted ERDA-6 (Test #1). The dashed lines indicate the "baseline" ranging from
845 0.1856 to 0.1902 mM Sr (duplicate measurements).

846

847

848

Information Only

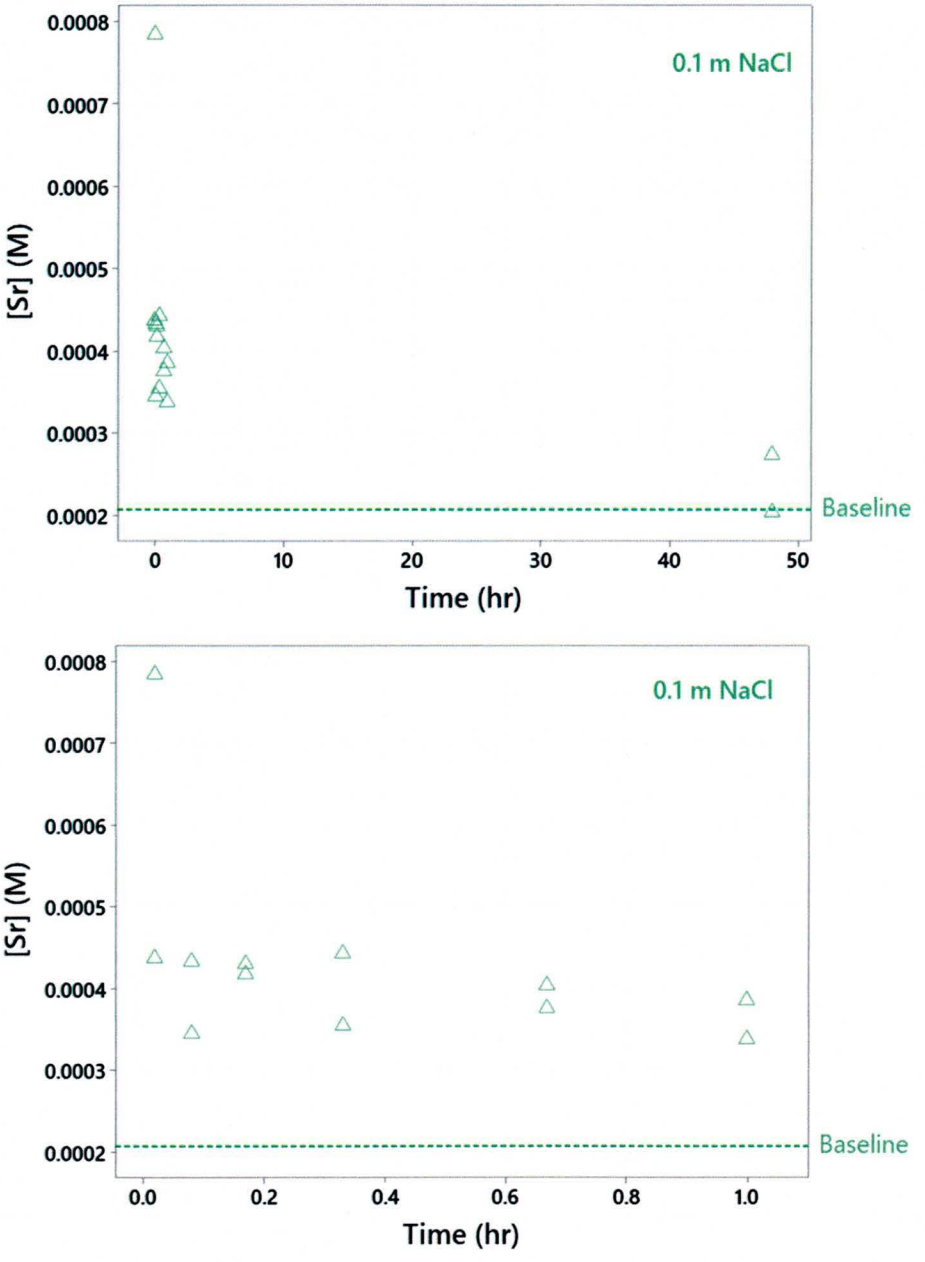

Figure B-9: Elemental strontium concentration over experiment duration (top) and over 1 hr (bottom) for strontianite in 0.1 m NaCl (Test #1). The dashed lines indicate the "baseline" ranging from 0.2074 to 0.2086 mM Sr (duplicate measurements). Note that after a slight decrease from the 0.02 hr (1 minute) mark, there is minimal change in concentration up to the second to last sampling point at 1 hour within the scatter of the data. The decrease from 0.02 to 0.08 hr (5 minutes) could indicate rapid settling of the larger (i.e., greater than colloid size) particles in the system or that the initial concentration of 0.7849 mM in reactor 8-1 is a potentially anomalous measurement.

Information Only

860

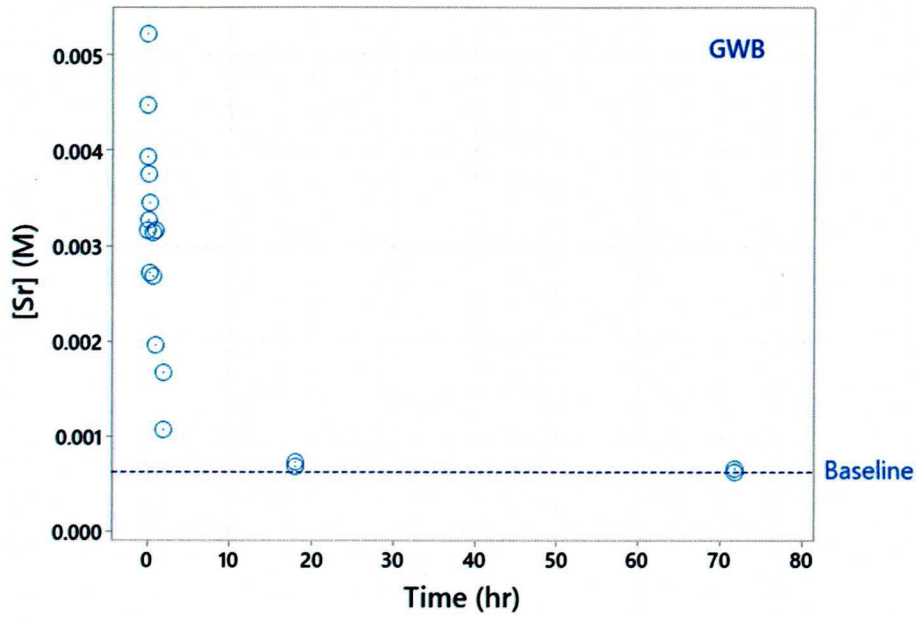

861

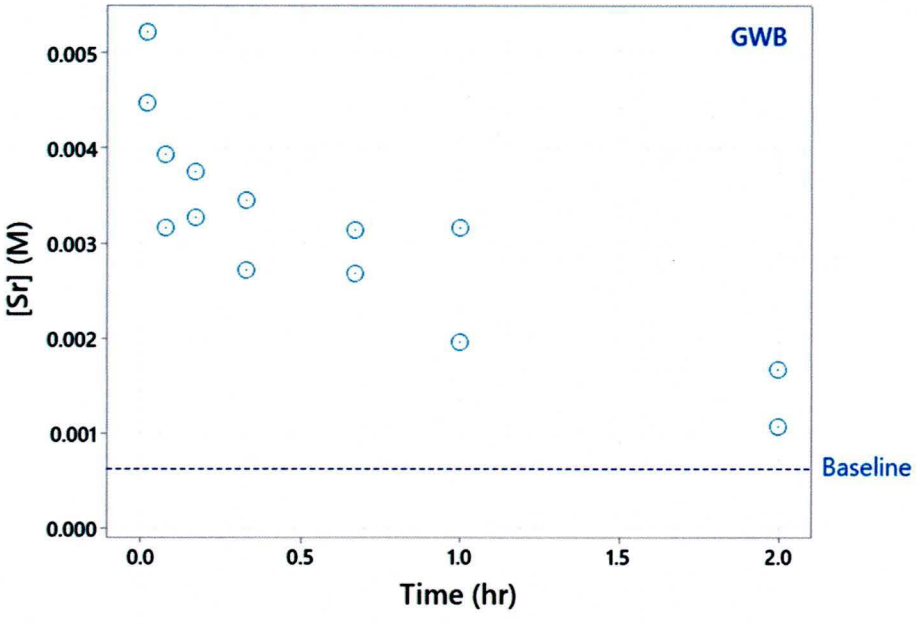

862 Figure B-10: Elemental strontium concentration over experiment duration (top) and over 2 hr (bottom) for
863 strontianite in GWB (Test #2). The dashed lines indicate the "baseline" ranging from 0.6306 to 0.6364
864 mM Sr (duplicate measurements).

Information Only

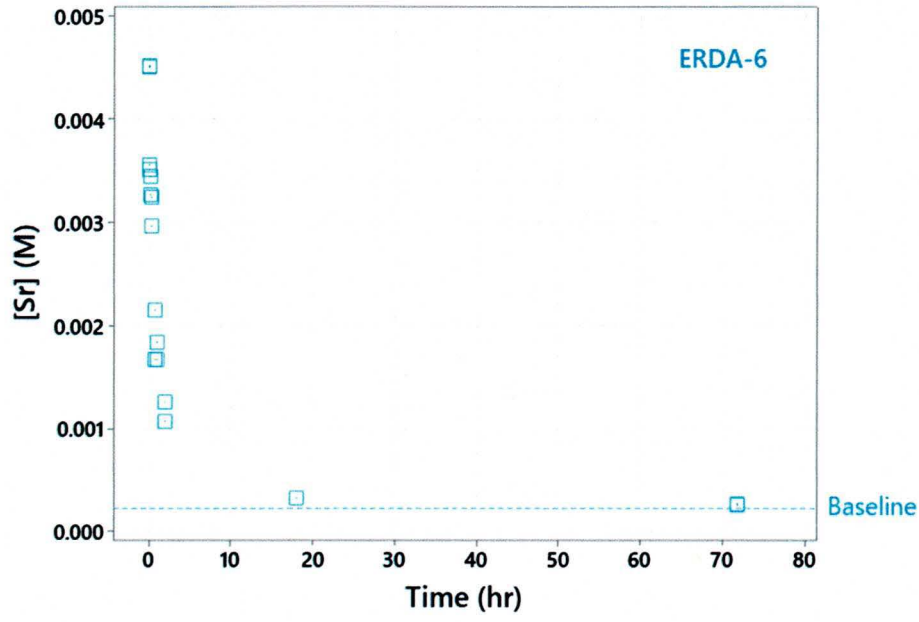

865

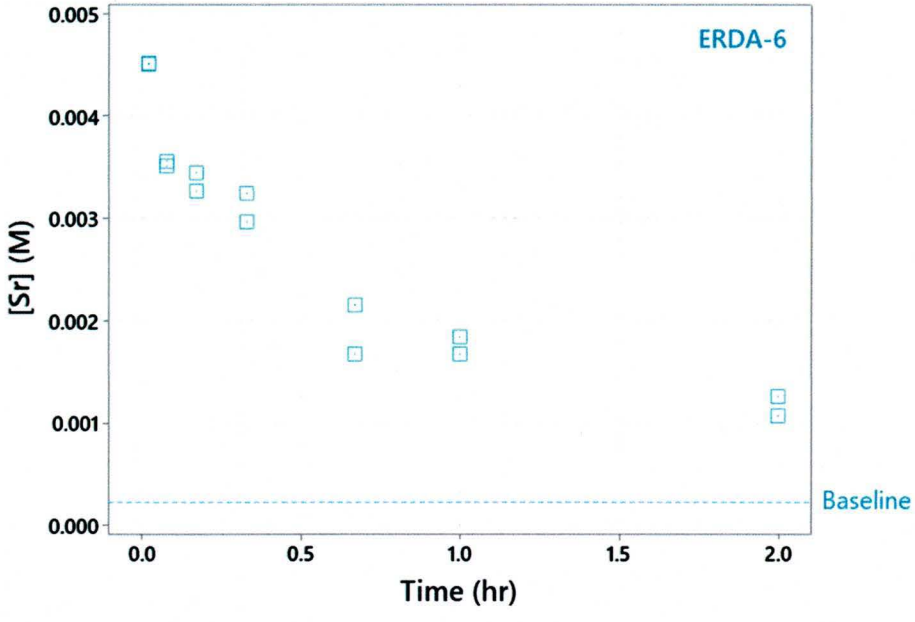

866

867 Figure B-11: Elemental strontium concentration over experiment duration (top) and over 2 hr (bottom) for
868 strontianite in ERDA-6 (Test #2). The dashed lines indicate the "baseline" ranging from 0.227 to 0.228
869 mM Sr (duplicate measurements).

870

Information Only

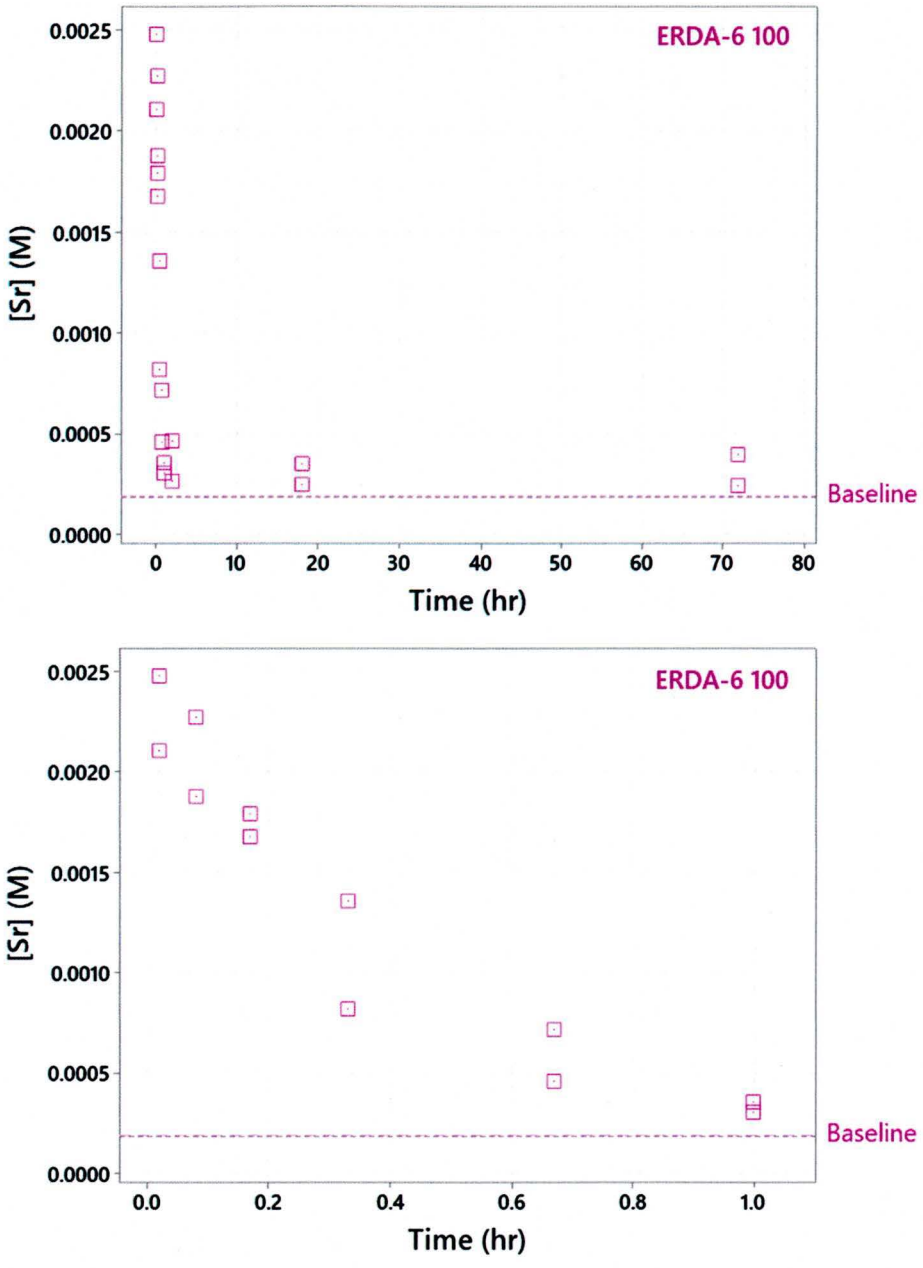

Figure B-12: Elemental strontium concentration over experiment duration (top) and over 1 hr (bottom)for strontianite in 100X diluted ERDA-6 (Test #2). The dashed lines indicate the "baseline" ranging from 0.1856 to 0.1902 mM Sr (duplicate measurements). Note the change in concentration between 1 hr and 72 hr appears negligible.

Information Only

878

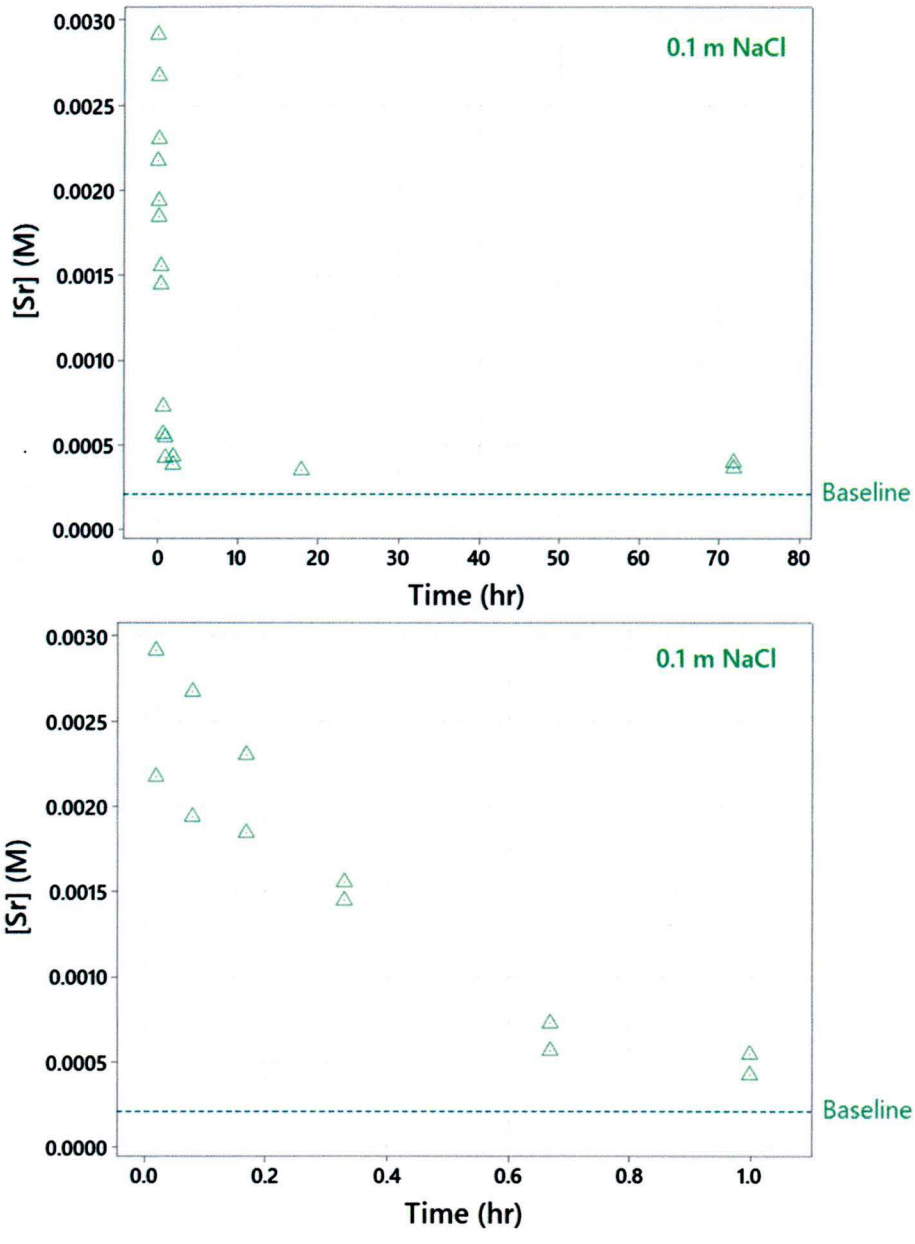

879

880 Figure B-13: Elemental strontium concentration over experiment duration (top) and over 1 hr (bottom) for
881 strontianite in 0.1 m NaCl (Test #2). The dashed lines indicate the "baseline" ranging from 0.2074 to
882 0.2086 mM Sr (duplicate measurements).

883

Information Only

9 *Appendix C: Initial calcite settling kinetics*

Linear regressions (

Figure C-1 is an example) were performed within the first hour of the experiment to capture the settling behavior of the particles given there was limited change in concentration after that period.

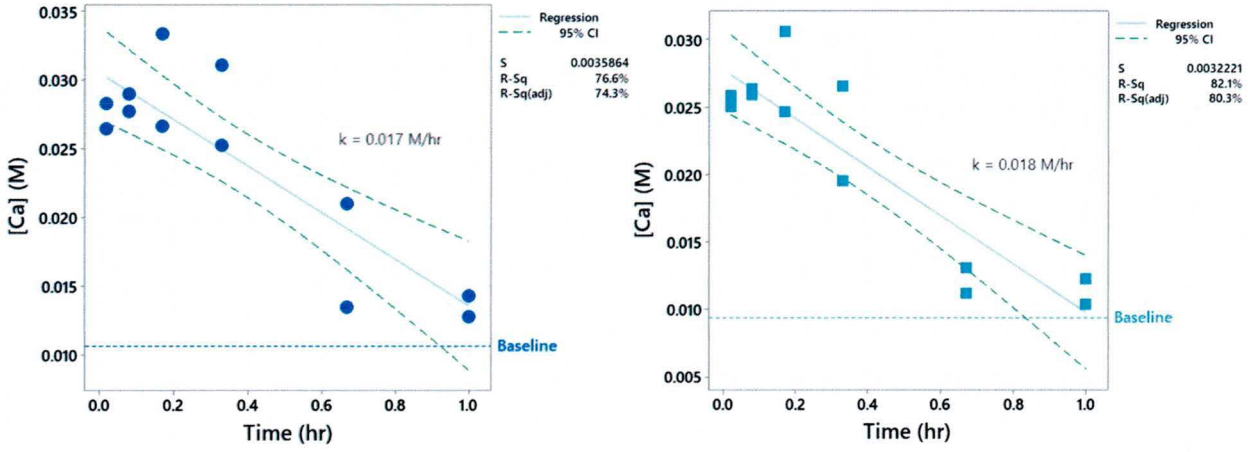

Figure C-1: Evaluating initial kinetics of calcite particle settling in GWB (left) and ERDA-6 (right). Solid lines represent linear regressions and dashed lines represent 95% confidence intervals. Note: different y-axes.

Table C-1 summarizes the results. 95% confidence intervals for respective slopes were calculated in Excel by multiplying the standard error of the slope by a two-tailed inverse of the Student's t-distribution with an alpha of 0.05 and n-2 degrees of freedom. R^2 represents the % of variation in mineral concentration that can be explained by the regression model. The rate constants exhibit no statistically significant difference even with increasing ionic strength and variable pH. Essentially, the results provide an indication of the overall experimental error. Half-lives were estimated by: $[Ca]_0/(2*k)$ and range from about 30 to 50 minutes.

Table C-1: Initial kinetics of particle settling

Mineral	Brine	Nominal I (m)	Nominal pH_{obs}	k ($M\text{-}hr^{-1}$ [a])	Est. $t_{1/2}$ (hr)	R^2
Calcite	NaCl	0.1	9.76	0.016 ± 0.007	0.5	71.5%
Calcite	ERDA-6	5.86	8.15	0.018 ± 0.006	0.7	82.1%
Calcite	SGWB	6.5	8.01	0.019 ± 0.005	0.5	89.6%
Calcite	GWB	8.25	7.45	0.017 ± 0.007	0.8	76.6%

Information Only

[a] Errors represent 95% confidence intervals associated with the regression slopes

901

Information Only